Global Dust Cycle and Direct Radiative Effect in E3SM Version 1: Impact of Increasing Model Resolution

Y. Feng[1], H. Wang[2], P. J. Rasch[2,7], K. Zhang[2], W. Lin[3], Q. Tang[4], S. Xie[4], D.S. Hamilton[5], N. Mahowald[5], and H. Yu[6]

[1]Environmental Science Division, Argonne National Laboratory, Lemont, IL 60439, USA
[2]Pacific Northwest National Laboratory, Richland, WA 99352, USA
[3]Brookhaven National Laboratory, NY 60439, USA
[4]Lawrence Livermore National Laboratory, Livermore, CA 94550, USA
[5]Cornell University, Ithaca, NY 14853, USA
[6]NASA Goddard Space Flight Center, Greenbelt, MD 20771, USA
[7]University of Washington, Seattle, WA, USA

Corresponding author: Yan Feng (yfeng@anl.gov)

Key Points:

(1) E3SMv1 captures spatial and temporal variability in the observed dust aerosol optical depth, but underestimates long-range transport.

(2) The net direct radiative effect of dust simulated by E3SMv1 is -0.42 Wm^{-2} with a smaller longwave warming than other recent studies.

(3) In addition to emission, dry removal of dust are highly sensitive to the increase of horizontal or vertical model resolution.

Abstract

Quantification of dust aerosols in Earth System models (ESMs) has important implications for water cycle and biogeochemistry studies. This study examines the global life cycle and direct radiative effects (DRE) of dust in the U.S. Department of Energy's Energy Exascale Earth System Model version 1 (E3SMv1), and the impact of increasing model resolution both horizontally and vertically. The default 1° E3SMv1 captures the spatial and temporal variability in the observed dust aerosol optical depth (DAOD) reasonably well, but overpredicts dust absorption in the shortwave. Simulations underestimate the dust vertical and long-range transport, compared with the satellite dust extinction profiles. After updating dust refractive indices and correcting for a bias in partitioning size-segregated emissions, both shortwave cooling and longwave warming of dust simulated by E3SMv1 are increased and agree better with other recent studies. The estimated net dust DRE of -0.42 Wm^{-2} represents a stronger cooling effect than the observationally based estimate -0.2 Wm^{-2} (-0.48 to +0.2), due to a smaller longwave warming. Constrained by a global mean DAOD, model sensitivity studies of increasing horizontal and vertical resolution show strong influences on the simulated global dust burden and lifetime primarily through the change of dust dry deposition rate; there are also remarkable differences in simulated spatial distributions of DAOD, DRE and deposition fluxes. Thus, constraining the global DAOD is insufficient for accurate representation of dust climate effects, especially in transitioning to higher- or variable-resolution ESMs. Better observational constraints of dust vertical profiles, dry deposition, size and longwave properties are needed.

Plain Language Summary

Dust aerosols affect Earth's climate through a myriad of pathways interacting with the global engery budget, atmospheric chemistry and biogeochemical cycles. It is critical for Earth system models to capture the global life cycle of dust aerosols for realistically quantifying the impact of climate change. As part of development of the U.S. Department of Energy's Energy Exascale Earth System Model Version 1 (E3SMv1), this study examines the representation of global dust life cycle and direct radiative effects in the recently released E3SMv1, resulting from both model physics improvements and increased model resolution. We find that the E3SMv1 model captures the spatial and temporal variations in the observed dust aerosols reasonably well, but underestimates the amount of dust advecting from desert sources to remote regions and from the ground to the upper atmosphere. Based on the model projection, dust aerosols insert a stronger cooling effect on Earth than previously estimated, after we use a better representation of dust particle size and absorption of sunlight. In addition, we show that not only dust generation but also removal and vertical transport of dust are highly sensitive to the model mesh size, thus need to be quantified in development of higher resolution models.

1 Introduction

Dust aerosols affect Earth's climate through direct and indirect impacts on the global energy budget. They can directly attenuate the incoming shortwave (SW) solar radiation by scattering and absorption (Tegen et al., 1996), and indirectly, modify cloud microphysical properties by acting as ice nuclei (DeMott et al., 2003) and cloud condensation nuclei (Rosenfeld et al., 2001), which change cloud albedo and thus affect the radiation balance. Despite being weak SW absorbers as individual particles, the abundant mass of dust in the atmosphere could cause a atmospheric heating that leads to changes of the lower troposphere thermal structure, cloud cover and liquid water path (Amiri-Farahani et al., 2017; Doherty & Evan, 2014). Additionally, dust absorbs in the infrared and longwave (LW) spectra due to unique characteristics of its mineral components (Sokolik et al., 1998). The LW effect of dust tends to cool the dust-laden layer and warm the air below, offsetting its direct SW warming effect within the atmosphere and cooling effect at the surface (Zhu et al., 2007). When deposited on snow or ice, dust particles can accelerate snowmelt by increasing the SW absorption similar to the effect of black carbon (Painter et al., 2012; Skiles et al., 2012). By perturbing the radiation energy balance, dust aerosols have further impacts on the large-scale general circulation (Evan et al., 2011; Lau et al., 2009; Miller et al., 2004) and regional precipitation (Solmon et al., 2015; Vinoj et al., 2014; C. Zhao et al., 2012; C. Zhao et al., 2011).

Other climate effects of dust occur through biogeochemical feedbacks and interactions with atmospheric chemistry. Dust particles deposited to the ocean surface are a major source of the essential micronutrients such as iron, which stimulate phytoplankton growth and nitrogen fixation in the high-nutrient low-chlorophyll sea waters (Jickells et al., 2005). Iron-enrichment driven by increased dust deposition could enhance the ocean uptake of atmospheric carbon dioxide (Hamilton et al., 2020), which is equivalent to inducing a negative climate forcing (Mahowald, 2011). Dust deposition also replenishes nutrient losses from soil and affects the health of terrestrial ecosystems (Yu, Chin, Yuan, et al., 2015). Additionally, dust plays a role in the gas-phase atmospheric chemistry and secondary aerosol formation by providing reactive surfaces for heterogeneous reactions with gaseous precursors (Dentener et al., 1996; Feng & Penner, 2007; C. Liu et al., 2013). Thus, it is critical for Earth system models (ESMs) to simulate the global life cycle of dust aerosols for both realistically quantifying the global energy balance and improved understanding of land-atmosphere-ocean couplings and feedbacks.

However, there are large differences in dust simulations among ESMs and between models and observations. Huneeus et al. (2011) compared 15 global dust aerosol models that participate the AeroCom model intercomparison project phase I (http://nansen.ipsl.jussieu.fr/AEROCOM/) with surface and satellite observations. An eight-fold difference was found in the present-day global dust emissions in the models, ranging from 514 to 4313 Tg yr^{-1}. The model differences in simulated dust burden and optical depth differ by a factor of four and five. The multi-model mean global dust AOD (DAOD) from the AeroCom models is 0.023, lower than an observationally constrained estimate of 0.030±0.005 (1σ) (Ridley et al., 2016). A few global modeling studies (Albani et al., 2014; Kok et al., 2014; Scanza et al., 2015) predict higher DAOD (0.03~0.033) in better agreement with the observations, mainly due to improved dust emission parameterizations and more representative SW refractive indices. But large uncertainties still exist in the CMIP6-type simulations of global dust cycles (A. Zhao et al., 2021), compared with satellite observations (Wu et al., 2020) or reanalysis products (Kok et al., 2021), even near the major dust source regions (Adebiyi & Kok, 2020; Evan et al., 2014; Kim et al., 2014; Wu et al., 2020). For dust properties, which either lack direct observational constraints (e.g., emissions), or depend on model representation of aerosol vertical profiles (e.g., dust surface concentration and deposition), the inter-model spread tend to be greater.

Uncertainties associated with modeled dust mass loadings and properties affect the assessment of dust radiative and other climatic effects. The net (SW+LW) direct radiative effect (DRE) of dust ranges from -0.5 to +0.35 W m^{-2} in recent literature (Di Biagio et al., 2020; Kok et al., 2017; Li et al., 2021; Scanza et al., 2015), while some earlier studies have reported larger negative estimates (Choobari et al., 2014; Forster et al., 2007; Miller et al., 2006; Woodward, 2001). In particular, dust DRE is very sensitive to the dust size distribution in models (C. Zhao et al., 2013). Kok et al. (2017) showed that the global DRE of dust is about a factor 2 less cooling than previous estimates (decreasing from -0.46 to -0.20 W m^{-2} in their estimate), when the size-resolved dust loadings are constrained by emitted dust size distribution and lifetime. Di Biagio et al. (2020) found that the inclusion of giant particles (≥20 μm) in models could have further weakened the dust cooling effect. Compared to the direct effect, the indirect effects of dust as ice nuclei or cloud condensation nuclei are less understood (DeMott et al., 2010). Dust perturbation on the cloud glaciation processes is not well understood and parameterized with less constraints in large-scale models (DeMott et al., 2015; Fan et al., 2014; Lohmann & Diehl, 2006).

Biogeochemical effects associated with uncertainties in dust iron deposition input to ocean biogeochemistry models vary by one order of magnitude among the CMIP5 models (Tagliabue et al., 2016). Moreover, the ESM-simulated iron deposition fluxes may be an order of magnitude smaller than what the more detail iron processing models suggest (Hamilton et al., 2022).

The present study evaluates the global life cycle and direct radiative effects of dust simulated by the U.S. DOE Energy Exascale Earth System Model version 1 (E3SMv1) (Golaz et al., 2019). E3SMv1 was built upon CESM1.0 (Neale et al., 2012) with significant improvements in the atmospheric physics and new ocean and sea ice models. It is generally used at a higher vertical and horizontal resolution compared to CESM1.0. The atmospheric component of the E3SMv1 (EAMv1) (Rasch et al., 2019; Xie et al., 2018) uses a higher vertical resolution (72 layers) than its predecessors, and is often configured in the horizontal globally at ~100km (ne30) as the standard (or low) resolution, or ~25km (ne120) as the high resolution. In comparison, the atmosphere component of CESM1.0, e.g., CAM5, has a coarser default resolution of 2° horizontally and 30 vertical layers (Neale et al., 2012). Increasing model resolution in E3SMv1 has had large impacts on clouds and precipitation (Xie et al., 2018). Previous studies have shown strong sensitivity of dust generation to increased horizontal resolution (Ridley et al., 2013). Coarse resolution can lead to underestimation of dust emissions by not resolving smaller scale wind variability (K. Zhang et al., 2016). On the other hand, increasing horizontal resolution also modifies the aerosol long-range transport and atmospheric burden, by better accounting for the spatial inhomogeneity in cloud and precipitation (Ma et al., 2015).

None of the previous studies we cited have examined the combined effects of increasing model horizontal grid spacing on global dust life cycle through changes in both emissions and removal, and consequently, the impact on DRE. It is unclear what other dust processes in addition to emission are scale-dependent and need to be calibrated for the ESMs moving into higher- or variable- resolution models. Vertically, increasing the number of model layers has been suggested to improve finer dust vertical features near sources (Teixeira et al., 2016) as well as its intercontinental transport (Eastham & Jacob, 2017), but the effect of increasing vertical model resolution on global dust budget and distributions has not been quantified. In addition, the EAMv1 includes a number of updates on aerosol physics (Wang et al., 2020), e.g., aerosol resuspension

after the re-evaporation below precipitation/clouds, which may have an impact on the coarse-mode aerosol simulations including dust.

The manuscript is organized as follows. Section 2 describes the dust aerosol scheme in the EAMv1, modeling experiments, and observational datasets used for model evaluation. It is followed by the model evalution against various observations in Section 3 that primarily focus on the results from the low-resolution E3SM model configuration with different dust properties. Section 4 presents the dust simulations and direct radiative effects with both the low and high EAMv1 resolutions, compared with other global models. Model sensitivity to the resolution changes is discussed. Finally, a summary of the main findings is given in Section 5.

2 Methodology

2.1 Dust and aerosol module

The E3SMv1 is a fully coupled ESM (Golaz et al., 2019). Dust-related processes are represented in EAMv1 and the land model component. Total emission fluxes of dust particles are calculated at each model time step following the wind erosion dust scheme by Zender et al. (2003). It depends on the surface wind speed, soil erodibility and a threshold friction velocity. Only the fraction of calculated emission flux of dust particles with diameter $\leq$ 10 μm is represented and simulated in EAMv1, as the coarser particles are currently assumed to fall onto the ground quickly and thus, not leave the grid cell where they are emitted. Although recent studies suggest that giant dust particles (e.g., >70 μm) may travel long distances (Does et al., 2018) and contribute to global dust loadings (Adebiyi & Kok, 2020), mechanisms for such long range transport of coarse dust particles remain poorly understood and it is not accounted for in E3SMv1 in the present study. The EAMv1 aerosol module (Wang et al., 2020) is developed from the four-mode version of the Modal Aerosol Module (MAM4) (Liu et al., 2016). It simulates internally mixed major aerosol compounds (sulfate, black carbon, primary and secondary organic matter, dust, sea salt and marine organic aerosols) in three size modes including Aitken, accumulation, and coarse modes, with an additional primary carbon mode representing freshly emitted black carbon and primary organic matter. In each aerosol size mode, mass concentrations of aerosol compounds and a total number concentration of aerosol mixture are calculated at each model time step and evolve in time. It is worth mentioning that although not included here, an interactive gas-phase chemistry is developed

(Tang et al., 2021) and available in EAM version 2, allowing the future coupling of dust aerosols with the gas-phase chemistry.

Dust is represented in both the accumulation and coarse aerosol modes following emission. The default EAMv1 uses the aerosol size distribution from Zender et al. (2003) to estimate the fractional dust emission fluxes within the (0.1-10) μm size range in diameter (87% of the total emissions) and then distribute the mass between the accumulation (3.2%) and coarse (96.8%) modes, respectively. In this study, we also examine a different dust emission size distribution (Kok, 2011), which predicts more particles in larger sizes, consistent with the recent measurements (Kok et al., 2017). The new size distribution assigns a smaller fraction of the total particle fluxes relative to the default model, about 73% of total mass to the (0.1-10) μm size range. The calculated fractions of the accumulation- and coarse- mode dust mass fluxes further shift the emitted particle size spectra toward larger sizes: about 1.1% in accumulation mode and 98.9% in coarse mode. Dry and wet removal of dust are treated as in CAM5.3 (Liu et al., 2012). A new treatment of aerosol resuspension is used in EAMv1 (Wang et al., 2020) compared to from CAM5.3. The new resuspension parametrization accounts for the release of large-size aerosol particles from evaporated raindrops and then adds them back to the coarse mode. As a result, it increases dry deposition of coarse-mode aerosols that are primarily dust and sea salt aerosols (Wang et al., 2020).

Aerosol optical properties are calculated following Ghan and Zaveri (2007) that assumes the volume-mean internally mixed aerosol species. In the released EAMv1, the default SW optical properties of dust are taken from the OPAC package (Hess et al., 1998). In this study we replace them with the observationally based dust optical properties derived from the AERONET measurements (Dubovik et al., 2000). Figure 1 compares the two sets of imaginary dust refractive indices as a function of wavelength. As shown, the AERONET-based imaginary indices are much lower (i.e., less absorbing) than the default sets for dust aerosols, which subsequently affect the calculated dust radiative effects. The LW absorption of mineral dust is treated as in CAM5 (Liu et al., 2012). Aerosol scattering in the LW is neglected in the current model, although this might result in some underestimation of dust LW warming (Dufresne et al., 2002). Dust DRE is calculated as the difference in the instantaneous fluxes at the top of the atmosphere (TOA) between two radiative transfer calculations at each model time step: one with all the aerosol species, and the other with all the aerosol species excluding dust. Both radiation calculations are carried out

under the same meteorological conditions (Ghan et al., 2012). The Rapid Radiative Transfer Model for GCM (RRTMG) is used for both SW and LW radiative transfer (Iacono et al., 2008).

2.2 E3SM simulations

Table 1 lists the E3SMv1 model simulations performed. All the simulations employ prescribed sea surface temperature (so called " F-compsets"), and are driven by the IPCC AR5 year 2000 anthropogenic aerosols emission inventories representative of the present-day. Specifically,

(1) LRes (the control run): represents the last 10-year results of a 11-year free-running simulation with the default EAMv1 configuration (~1° and 72 layers). This is used as the EAMv1 control run for examining the global dust cycle and direct radiative effects compared with other global models and the sensitivity experiments with EAMv1;

(2) LResT: is similar to (1), and uses the different dust size distribution and SW absorption properties described above (Letter "T" stands for "This study"). Comparison of (2) with (1) will show the impact of the updated dust properties on the simulated dust distribution and DRE;

(3) LResT-Ndg: is similar to (2). Rather than in a free-running mode, this run is nudged to the ECMWF reanalysis temperature and wind for 2009 and 2010 ("Ndg" stands for "Nudging"). The 2010 results were analyzed. Comparison of (3) and (2) will show the impact of nudging to the reanalysis meteorology, in particular, on spatial and temporal correlations with the surface observations;

(4) LResT-Ndg-HRtuned: is similar to (3), configured with the high-resolution tuning parameters for atmospheric physics (Caldwell et al., 2019), in which some of the parameters relevant to cloud and convection are re-tuned to achieve TOA global radiative energy budget balance and improve cloud and precipitation simulations ("HRtuned" stands for "High-Resolution tuned"). Comparison of (3) and (4) can inform how does the high-resolution parameter tuning affect the low- and high- resolution E3SM simulations of dust;

(5) HRes (High Resolution): is a 5-year run of the high-resolution E3SMv1 (~0.25° and 72 layers) and the last 4 years were used for analysis. This HRes simulation uses the same atmospheric physics package as in the default high-resolution E3SMv1 (Caldwell et al.,

2019). Here, more output fields are saved for understanding the dust processes sensitive to resolution in comparison with (1) LRes. Given limited computational resources, we performed 5-year HRes simulations, and used the last 4 years to compare with the LRes simulations for the same time period (years 2-5). There might be noise in some model-predicted mean states that are affected by slow processes such as in the stratosphere, but the main use of this sensitivity study is to compare DAOD, dust vertical distribution in the troposphere, and deposition fluxes at surface between the low and high resolutions. These fields are all related to fast physics, e.g., as shown in Section 4, the global dust lifetime is ~2 days and at the regional scale, the lifetime is < 50 days over most of the domain. Therefore, the 4-year averages are sufficient to show the correspondence of these dust fields and the processes related to the resolution changes;

(6) LResZ30: is the last 5-year averages of a 6-year free-running simulation configured with the low horizontal grid spacing (~1°) same as (1) LRes, using a coarser vertical resolution of total 30 vertical layers. Similar to (5), the 5-year averages from LResZ30 are reasonable to compare with the years 2-6 results from (1) LRes for understanding the model sensitivity to the vertical resolution change;

(7) LResT-HRtuned: is a 2-year calculation of dust DRE with the low-resolution configuration same as (2) LResT, using the high-resolution tuning parameters. This sensitivity experiment is used to compare with (8), the high-resolution simulation below, for examining the sensitivity of dust DRE to the increase of horizontal resolution while excluding the influences from the high-resolution parameter tuning;

(8) HResT: is similar to (7) with the high-resolution configuration (~0.25° and 72 layers). The DRE calculations require more computional resources especially for the high resolution, so we performed a 2-year simulation with HResT. The last-year results from the 2-year simulations were analyzed for both (7) and (8). Although there might be noise due to interannual variability in the calculated DREs, we limit discussions to the differences between the two resolutions, both of which are under the same influences and driven by those fast processes responding to the resolution changes discussed in (5). The global DAOD in (7) and (8) is tuned slightly higher at 0.04 than LResT at 0.03 to obtain a global

AOD ~0.14 similar to the observations, while the DAOD is still within the observationally based estimate of 0.03±0.01 (Kok et al., 2017).

Since there are no direct constraints of global dust emissions from observations, the annual and global mean DAOD in all the model simulations with E3SMv1 is constrained to 0.026~0.04 (Tables 1), approximately matching the observationally based estimate of 0.03±0.01 (Kok et al., 2017), by tuning the emission parameter, i.e., the global scaling factor. As a result, global dust emissions and deposition fluxes are adjusted to a similar level in each set of the sensitivity simulations, independent of model resolution or model physics. We discuss the impact of this emission tuning approach on the simulated dust distributions and DRE in Section 4.

2.3 Observational Datasets

Evaluation of dust life cycle focuses on the DAOD and absorption AOD (AAOD), vertical profiles, and deposition fluxes: the first three are key properties for calculating the DRE, while deposition fluxes are linked to the role of dust as nutrient supply to remote terrestrial and ocean ecosystems. In this study, AOD and AAOD observations are taken from the AERONET Level 1.5 daily data products between 2006 and 2015 based on the Version 3 Direct Sun and Inversion Algorithms (Dubovik & King, 2000; Dubovik et al., 2000). Monthly mean AOD is calculated from the daily data for sites with measurements for more than 10 days per month. The yearly means of AOD are then calculated from the monthly averages for sites with more than 10 months of data per year and averaged over the 10-year period (2006-2015) to compare with the model simulations. In addition, a total of 19 'dusty' AERONET sites listed in Table 2 are identified by selecting the sites over land which have a multi-year mean Ångstrom Exponent (AE) < 0.8. Using this criterion, the simulated dust AOD at all the selected sites except for Trelew in South America contributes more than 50% of the total AOD, suggesting that these sites are heavily influenced by dust aerosols; therefore, the model-observation comparison of total AOD and AAOD at these locations are indicative of the model performance in simulating dust.

The CALIOP (Cloud-Aerosol Lidar with Orthogonal Polarization) V4 Aerosol Profiles between 2009 – 2012 are used to evaluate the model dust vertical profiles. Seasonal mean aerosol extinction profiles (Mm^{-1}) are calculated from the CALIOP nighttime product covering most of the source and downwind regions of the Sahara Desert (latitude: 19°S to 49°N, and longitude: 97.5°W to 57.5°E) from June to August (JJA) and December to February (DJF). Dust particles are

largely coarse sized and non-spherical in shape, resulting in a much larger depolarization ratio than other aerosol types. Speciated dust extinction profiles are thus derived based on the CALIOP depolarization measurements (Yu, Chin, Bian, et al., 2015; Yu et al., 2019). The obtained dust extinction profiles are averaged between 0° and 30°N and for JJA and DJF. These profiles are then used to evaluate the seasonal and long-distance transport of dust and vertical distributions simulated by E3SM.

Observations of dust deposition fluxes for the modern climate were estimated from the global data set compiled by Albani et al. (2014) which combined multiple observational sources such as ice core, marine sediments, and terrestrial deposits to provide a global distribution of climatological annual mean dust deposition fluxes. The uncertainty associated with this deposition flux data is discussed in Albani et al. (2014). At the minimum, it provides observational constraints of the geographical pattern and regional variability in dust deposition fluxes.

3 Model Evaluation

This section focuses primarily on the behavior of the low-resolution standard configuration with different choices of model physics (LRes, LResT, LResT-Ndg, and LResT-Ndg-HRtuned). Sensitivity to the model resolution is discussed in Section 4.

3.1 AOD and AAOD

All the E3SMv1 low-resolution simulations yield a similar global DAOD about 0.026-0.029. At the regional scale, Figure 2a shows that the control run LRes predicts the highest DAODs (>0.5) over the major dust source regions including Sahara, Arabian Peninsula, the Gobi and Taklimakan deserts in Asia, and the Australian deserts. Over the remote oceans and within the high latitudes, the modeled DAOD generally falls into the 0.005 to 0.01 range, except for plumes downwind of major dust sources where higher predictions of DAOD close to 0.1 are obtained. Also shown in Fig. 2a, dust aerosols are more prevalent in the Northern Hemisphere than in the Southern Hemisphere in terms of both source strengths and long-distance transport potential.

Although global DAOD is similar among the model variants, the dust distributions are different and sensitive to the model dust properties and meteorological conditions. Fig. 2b shows that LResT produces higher DAODs than LRes over some of the dust source regions such as E Asia and Australia and lower predications in the downwind and remote regions. This is because

LResT uses a size distribution predicting more coarse particles upon emission (Kok, 2011) that leads to more dry deposition near the sources and thus less aerosol transport over long distances. On the other hand, emissions are increased, under the global DAOD constraint, to compensate for the enhanced deposition that result in higher DAODs near the sources with LResT. Therefore, LResT attributes a larger fraction (85%) of the global DAOD to the coarse-mode particles (diameter > 1μm) than LRes (66%). Regionally, this pattern is more evident (Fig. 2c and 2d) that the coarse-mode dusts in LResT dominate the simulated DAOD over 60% in most of the dust-influenced regions even far away from the sources. For the same DAOD, since coarse-mode dust particles result in larger LW warming and less SW cooling than the fine particles, this change of dust size distribution would lead a less cooling net effect of dust in LResT (Di Biagio et al., 2020; Kok et al., 2017).

The predicted spatial distribution of DAOD is also sensitive to the model meteorology. Forced by the ERA reanalysis data, LResT-Ndg in Fig. 2e shows weaker long transport of dust indicated by the lower DAOD values in the remote regions compared with LResT in Fig. 2b, due to the enhanced removal. Regional DAODs are also affected by the modified dust emissions, for example, the high-latitude DAOD associated with the Antarctic dust in LResT is not simulated by LResT-Ndg, because the surface (10-meter) windspeeds from the reanalyses in year 2010 used by LResT-Ndg are lower than the model-simulated winds for dust mobilization in Antarctic (Fig. S1 and Fig. S2). We will further examine the impact of nudged meteorology on simulated dust spatial distributions in comparison with the AERONET observations below. The high-resolution parameter tuning could also potentially affect the dust simulations through changing the simulated meteorological conditions. As shown in Fig. 2f, compared to LResT-Ndg, LResT-Ndg-HRtuned simulates slightly weaker dust transport, thus smaller DAODs over the remote oceans. It also affects the DAOD distribution by modulating dust mobilization, e.g., over Antarctic (Fig. S1), through the impact on dry convective eddies over land from the high-resolution parameter tuning that may change the surface wind variability. This sensitivity experiment shows that differences in dust simulations between the E3SM low- and high- res simulations (i.e., LRes and HRes in

Section 4) may be also attributable to the tuning parameters, although the contribution is small (Fig. S3) except for a few spots.

The simulated annual mean AOD and AAOD over the selected dusty sites are compared with the AERONET observations in Figure 3. Table 2 lists the site-specific information and calculated mean statistics. Since most of these dusty sites are located over or near the major source regions in the northern hemisphere (denoted by gray solid circles in Fig. 2a), the annual averages of the site-specific AERONET AOD are high: above 0.4 in the low latitudes (<15°N) and above 0.15 in the subtropics (<30°N). Most of these high AOD values from AERONET are captured in LRes, with a multi-site mean AOD of 0.34 and a spatial correlation coefficient of 0.77. Like LRes, simulations of LResT and LResT-Ndg also generate similar annual mean AODs (0.34 and 0.33, respectively) and a strong spatial correlation with the AERONET AODs (correlation coefficients >0.7). This indicates that the DAOD changes resulting from different dust emission size distributions in LResT and LResT-Ndg reflect primarily on the long-distance transport potential of dust rather than changing the dust concentration over the source regions (Fig. 2). On the other hand, LResT and LResT-Ndg improve the AAOD predictions relative to LRes remarkably in comparison with the AERONET data, as shown in Fig. 3b. The simulated AAOD is reduced by a factor of two at nearly all the sites except for Trelew, where the E3SMv1 predicts very little dust (<2% of total AOD) probably due to the model low-biased soil erodibility, and thus AAOD is insensitive to the updated dust SW optics in LResT and LResT-Ndg. On average, the mean AAOD over the 19 AERONET sites decreases from 0.038 in LRes to 0.023 and 0.022 in LResT and LResT-Ndg, respectively, showing a great improvement compared with the AERONET mean at 0.017. Like AOD, the observed spatial variability in AAOD is also reproduced largely by LRes, LResT and LResT-Ndg with correlation coefficients > 0.7. Between LResT and LResT-Ndg, nudging to the ERA reanalyse meteorology for a single year (2010) by LResT-Ndg results in a weaker spatial correlation with the AERONET multi-year climatology than LResT, which represents the model-simulated climatology averaged over 10 years. It implies that the free-running E3SMv1 configuration simulates the spatial variability in meteorology that drives dust distributions near the sources reasonably well, but may overestimate the strength that leads to the

high-biased AOD (by ~+13%) and AAOD (by ~+35%) values compared with the AERONET multi-year means.

In addition to the yearly averages, seasonal variations of AOD simulated by LRes, LResT and LResT-Ndg are evaluated in Figure 4 for the 18 dusty sites (excluding the Trelew site where E3SM predicts a low dust concentration). Because the E3SMv1 uses a fixed soil erodibility map, seasonality in the calculated AOD is mainly driven by variations in the meteorological conditions that govern the emissions, transport, and residence time of dust in the atmosphere, such as surface winds, convection intensity, and precipitation. The monthly predictions of AOD by LRes and LResT in the free running configuration correlate reasonably well with the AERONET observations for representing the seasonality of dust loadings near the sources with the calculated correlation coefficients > 0.5 for 14 and 13 out of the 18 sites, respectively. Most of the 13 or 14 sites are located within the sub-tropical Northern Hemisphere between 15°N-30°N. In contrast, the calculated temporal correlations are relatively weaker at lower or higher latitidues; especially for the two low-latitude sites (IER_Cinzana and Banizoumbou), both LRes and LResT yield very low correlation coefficients (0.21~0.33). When nudged towards the ERA reanalysis meteorology in 2010, the simulated monthly variability in AOD at these two low-latitude sites improve considerably with LResT-Ndg, as the temporal correlation coefficients with AERONET increase by more than a factor of two (0.75 and 0.69); on the other hand, LResT-Ndg nudging to the single-year reanalyses (year 2010) does not outperform the climatology simulated by LRes or LResT at other sites systematically. This indicates that large uncertainty in the temporal variations of the lower-latitidue dust in E3SMv1 are associated with the model representation of the large-scale meteorology in those regions. On the seasonal scale, both the observations and model results yield the yearly maximum AOD near the sources approximately during the hemispheric summer, e.g., June-July-August (JJA), and shifting to an earlier peak in spring toward the equator, e.g., March-April-May (MAM), while the dust-influenced AODs are consistently the lowest during the hemispheric winter.

3.2 Vertical Distribution

In addition to the column integraged AOD and AAOD, vertical distribution of dust is an important property in the calculation of dust direct radiative effects, in particular for LW radiation flux. Figure 5 compares dust extinction profiles between 0° and 30°N derived from CALIOP and

three model experiments (LRes, LResT, and LResT-Ndg) for winter (DJF) and summer (JJA) months, respectively. The CALIOP dust extinctions at 532nm are derived from lidar backscatter signals and particulate depolarization ratios, which are intrinsically different from the bottom-up model calculations based on the dust mass loadings and mass extinction efficiency. The differences between the two approaches may lead to ambiguity in the direct comparison of dust extinction. For instance, in Figure 5b, the large extinction retrievals from CALIOP (30~40 Mm^{-1}) between 60°W to 80° W in the marine boundary layer might be subject to some retrieval uncertainties, such as cloud contamination, and the presence of non-spherical dry sea salt, which are not included in the model-simulated dust extinctions. Thus, the analysis below focuses more on comparing the vertical structure of dust distributions rather than absolute values.

The CALIOP extinctions show that the source-region dusts associated with strong convection ascend from the ground up to ~6 km in summer, which is about 2 km higher than during winter. All the E3SMv1 simulations capture such seasonal variations in the elevated dust layers, but underpredict the dust extinctions, especially in the free troposphere. These model low biases are greater in summer than in winter when dust is concentrated mostly in the lower troposphere (< 3-4 km). As a result of the underestimated vertical transport, E3SMv1 also predicts weaker long-range transport of dust westward from the African continent to the tropical/subtropical Atlantic Ocean, compared to the satellite observations (Fig. 5). This indicates that both the vertical transport and removal efficiency of dust in E3SMv1 may need to be re-calibrated to allow more efficient transport of dust in the long distances, as recent studies of aerosol dry deposition indicate that most aerosol models likely overpredict the particle removal compared with the new measurements (Emerson et al., 2020). With more coarser particles emitted, dust extinctions from LResT agree better with the CALIOP retrievals than LRes in the lower troposphere (<2km) near the sources, e.g., between 20°W-20°E. But the underestimation in dust transport is more substantial in LResT as coarser particles fall onto the ground more rapidly.

Over the major dust sources, both LRes and LResT in free-running configuration captures the high dust extinctions around 20°E, but underestimate the peak values around the 0° longitude revealed in the observations, especially in JJA. It is likely due to the model bias in underpredicting the surface winds for dust generation in those areas, as when nudged to the reanalysis meteorology, LResT-Ndg simulates higher dust extinctions near the surface and agrees better with the satellite

observations between 15°W and 0° in JJA. However, similar to the AOD comparison, LRes and LResT represent the multi-year averaged observations of dust extinction cross sections over the major sources between 0 and 30°N reasonably well, better than LResT-Ndg over a large spatial context.

3.3 Deposition

Dust deposition is a major supplier of the micronutrient iron from the atmosphere to the open ocean (Hamilton et al., 2022; Mahowald et al., 2009). It is thus important to quantify the uncertainty in dust deposition simulated in ESMs (Myriokefalitakis et al., 2018; Tagliabue et al., 2016). Figure 6 shows the global distribution of annual dust deposition fluxes predicted by LRes and LResT, along with a comparison with 108 climatology observations of dust deposition (LResT-Ndg is not shown here since it is nudged to the year 2010 meteorology not representative for comparion with the climatology data). The observational data taken from Albani et al. (2014) are overlaid and denoted by the solid circle symbols with the same color scale used for the model results in Fig. 6a and 6b. In general, large dust particles deposit quickly to the ground after emission through gravitational settling, yielding large deposition fluxes in the vicinity of the major dust source regions, such as the Saharan-Arabian region, deserts in Asia and Australia, and Patagonia. Compared to LRes, LResT predicts lower deposition fluxes over the remote North Pacific and North Atlantic Ocean, because of the reduced dust long-range transport associated with the coarser size distribution, while enhanced deposition is predicted downwind of the Australian dust sources over the South Pacific Ocean from increased emissions near the source regions. Since the dust deposition fluxes are calculated proportional to dust concentrations, the impact of different model configurations on spatial distribution of dust deposition fluxes is similar to DAOD as discussed for Fig. 2.

Fig. 6c compares the modeled deposition fluxes with the observations over the 108 locations. Most of the model results are within a factor of 10 with the observations, consistent with other global dust studies (Albani et al., 2014; Hamilton et al., 2019). The agreement between the model and data is slightly better over the dust-laden regions, indicated by less scatter and fewer outliners for the observed deposition fluxes larger than 1 g m^{-2} yr^{-1}. The regional mean differences between the model predictions and observations are summarized in Table 3. For the locations near the dust sources, such as N. Africa/subtropical NE Atlantic and Asia/Arabian Sea, LRes and LResT

475 overestimate dust deposition by about a factor of 2. The high biases in these two source regions
476 dominate the overall mean bias, although the deposition fluxes are underestimated over the remote
477 oceans, including the North and South Pacific Ocean by about 40-60% and South Atlantic by about
478 20-30%. In the Arctic and Antarctic regions, the observed dust deposition is very low, where the
479 model results have the highest relative biases, which are associated with the high-latitude dust
480 emissions (i.e, in Antarctic) as well as the mid-latitude dust transport. However, the observational
481 data in high latitudes are derived from measurements with great uncertainty, e.g., from ice core,
482 especially for quantifying the present-day dust deposition fluxes. Over all the regions, simulations
483 of LRes and LResT show similar biases (Table 3), either high or low, indicating that the updated
484 dust emission size distributions in LResT do not help much in resolving the model-observation
485 discrepancies in the deposition fluxes. Other factors that could promote transport of dust to the
486 remote regions, for example via revisions to aerosol dry and wet deposition efficiency as well as
487 particle sphericity in calculating settling velocity, may be worth further investigation.

488 **4. Results**

489 **4.1 Global Budgets and Impact of Increased Model Resolution**

490 Table 4 compares the global budgets of dust predicted by E3SMv1 with other modeling
491 studies. For the three low-resolution simulations (LRes, LResT, and LResT-Ndg), dust emissions
492 range from about 4700 to 5400 Tg/yr, higher than CAM5 and other global models listed in Table
493 4, although the observations do not provide a strong constraint on global dust emissions and
494 deposition. Among the different E3SM configurations, LResT and LResT-Ndg require higher dust
495 emissions than the default LRes, because they predict more coarse-mode dust that deposits rapidly
496 to produce a similar AOD, thus requiring more particles emitted to retain the dust loading in the
497 atmosphere. This is more consistent with a recent study (Kok et al., 2021), which estimates a global
498 emission flux of dust greater than current models, approximately 5000 Tg/yr, since it accounts for
499 more coarser dust particles with diameter up to 20 μm. The size differences also lead to higher
500 dust burdens in LResT and LResT-Ndg than in LRes, because coarse-mode dust scatters the
501 sunlight less efficiently than fine-mode dusts and higher dust loadings are needed for matching the

DAOD constraint. On the other hand, the global dust burden simulated by LRes is similar to CAM5, which uses the same dust size partitioning upon emission.

Dry (or wet) deposition rate (or loss frequency), defined as the ratio of dust dry (or wet) deposition flux (Tg/yr) divided by its mass burden (Tg) in unit of day^{-1}, is often used to quantify the model-simulated dry (or wet) deposition efficiency, rather than absolute deposition fluxes, since the former is not sensitive to the resolution-dependent dust emissions. In the low-resolution E3SMv1 (LRes, LResT and LResT-Ndg), dust dry deposition rate is more than 3 fold greater than the wet deposition rate, indicating that globally, the removal of dust occurs preferentially through dry deposition than wet deposition for their large particle size and low hygroscopicity. Despite different absolute deposition fluxes, three low-resolution E3SMv1 configurations simulate similar dry and wet deposition rates for dust aerosols. Dust lifetime, which is equivalent to the inverse of the total deposition rate, is also loosely dependent on the model dust properties (i.e., size distribution), within 1.7-1.9 days for LRes, LResT and LResT-Ndg. This estimated lifetime is shorter than the typical range of CAM5 (2.6 days) and the AeroCom modeling studies (4.14±43% days), mainly driven by the larger dust dry deposition rate of E3SM, which is about a factor of two higher. The wet deposition rate of E3SM is similar to CAM5 slightly overestimated compared to other modeling studies (Liu et al., 2012). The predicted strength of dust deposition especially through the dry removal and the short lifetime imply that the low resolution E3SMv1 likely underestimates the vertical transport of dust to the free troposphere. This is consistent with the comparison of the E3SM-simulated extinction profiles with the satellite observations in Section 3.2.

Without tuning the dust emission parameters, increasing the model horizontal resolution by a factor of 4 from the E3SMv1 low resolution (~100km) to the higher resolution (~25km) simulation results in about a 29% increase of global dust emission fluxes from 4702 to 6044 Tg yr^{-1}, and the global DAOD is increased by 42% from 0.026 to 0.037. This is essentially due to the non-linear strong dependence of dust emissions on the resolved small-scale surface winds (Ridley et al., 2013; K. Zhang et al., 2016). In particular, DAOD shows a stronger dependency on the resolution than emissions, indicated by a larger percent increase. The additional DAOD increase is a result of the weakened dry removal (especially turbulent deposition) of dust at higher horizontal resolution, although there is also a small enhancement in wet removal from the better-

resolved clouds and precipitation (Ma et al., 2015). The strong sensitivity to resolution exhibited in the global DAOD suggests that both dust emission and deposition parameterizations are highly resolution- or scale- dependent. In the standard E3SMv1 high-resolution configuration (HRes), dust emissions are adjusted to match the global DAOD constraint of 0.03. After the adjustment, HRes simulates the global dust emissions and DAOD similar to LRes, but the finer horizontal resolution of HRes leads to a ~17% lower dry deposition rate and slightly higher wet deposition rate. As a result, the dust lifetime in the HRes simulation increases to 2.1 days, more comparable to other models than LRes at 1.85 days.

In addition to the increased horizontal resolution, the standard E3SMv1 also has a finer vertical resolution with 72 layers compared to its CAM5 predecessor with 30 layers. To examine the effect of increasing the number of vertical layers, one E3SMv1 simulation (LResZ30) was conducted with the same 30 vertical layers as CAM5 (Liu et al., 2012). Constrained by the same global DAOD, LResZ30 generates higher dust emissions than CAM5 for higher horizontal grid spacing, but to a lesser extent compared to LRes. The primary factor determining this difference from LRes is the lower dry deposition rate of dust simulated by LResZ30, which decreases to 0.29 day^{-1} by 33% from 0.43 day^{-1} in LRes. The reduction of dust dry deposition also leads to a longer dust lifetime at 2.4 days. This sensitivity model experiment of decreasing the E3SMv1 vertical resolution reveals similar effects on the simulated dust burden and lifetime to the model refinement of horizontal resolution, although the underlying mechanisms may be different. For example, both gravitational settling and turbulent deposition responsible for dust dry removal are influenced equally by changing the vertical resolution, while increasing horizontal resolution has a larger impact on the latter, resulting in a larger contribution of gravitational settling of dust in total dry deposition (from 75% in LRes to 78% in HRes). In contrast to dry deposition, refining the model resolution, either horizontally or vertically, has moderate effects on the dust wet deposition rate globally, although it could be more significant on the regional scales and for hygroscopic aerosol species such as sea salt or sulfate aerosols (Caldwell et al., 2019).

The comparison of global dust budgets with different E3SMv1 configurations suggests that the global mean DAOD does not fully constrain the life cycle of dust. When constrained by the same DAOD, the model diversity in global emissions, deposition, burden, and lifetime of dust between E3SM configurations and other models are evident, as summarized in Table 4. These model disagreements imply a wide range of differences in dust transport and spatial distributions

that could further influence the direct and indirect radiative effects of dust. Therefore, it is important to understand the contributing processes to the inter-model differences in dust global budgets and the manifested impact. Sensitivity of the dust simulations to dust emission size distribution and SW optics (between LRes and LResT) has been discussed in Section 3 compared with the observations. Here we further examine the impact of increased model resolution both horizontally and vertically on individual dust proccesses.

4.2 Effects of Increasing Resolution on DAOD

Figure 7 shows the global distributions of annual mean DAOD, emissions, and lifetime simulated by HRes, and their differences from LRes. HRes simulates the geographical pattern and hemispheric contrast of annual DAOD similar to LRes (Fig. 2a), however, there are great differences in their reginal DAOD values; as shown in in Fig. 7b, the DAOD differences between the two simulations vary by region in both sign and magnitude. HRes generally predicts higher DAODs over the major dust source regions (>25%) than LRes as well as the adjacent oceans downwind of the dust transport. In particular, over the Arabian Pennisula, Middle East, and Taklimakan desert in E Asia , the DAOD predictions in HRes are more than doubled relative to LRes. These regional increases of DAOD are compensated by lower predictions over the western Sahel, tropical/subtropic Atlantic, S. America and Europe, adding up to a similar global mean DAOD between HRes and LRes. Such large positive or negative changes in DAOD ($>\pm0.1$) could potentially affect the simulated regional radiation balance and hydrological cycle. They are driven by the compound effects of changes in dust emissions and deposition rate.

The HRes simulation of dust emissions and the differences from LRes are illustrated in Fig. 7c and 7d. Emission fluxes in the dust source regions generally increase with higher model horizontal resolution as expected for HRes, leading to larger local DAODs. However, some HRes grid cells are associated with lower dust emission fluxes than LRes, e.g., negative changes over North Africa, which contribute to the smaller DAOD in HRes over Europe and the southeastern Atlantic. The decrease of dust emissions from LRes to HRes is due to a larger global scaling factor used in HRes to scale the total emissions down to the LRes level; in those grid cells, the increase of emissions due to the resolved surface winds are smaller than the decrease of emissions resulting from the global scaling. These regionally different responses in dust emissions, resulting from the empirical global tuning approach, would alter the relative contributions of dust from the various

sources. For example, dust emissions from the Middle East and E Asia will constitute a larger fraction in the global emission fluxes in HRes than in LRes because of its increased dust mobilization, while the North African dust emissions decrease. Subsequently, it would change the spatial distributions of simulated dust loadings, DAOD, and radiative effects, because dust transport is influcenced by the regional meteorology and dust properties such as size and mineral composition are source-dependent.

In addition to the emissions, global distributions of dust burden and DAOD are also influenced by the dry or wet removal (deposition) processes represented in LRes and HRes. To understand the resolution effect on deposition, dust lifetime (day), which is the inverse of deposition rate (day^{-1}) and insensitive to the column dust burden, simulated by HRes and the changes from LRes are shown in Fig. 7e and Fig. 7f, respectively. Although the globally averaged dust lifetime is short ~2-4 days, dust deposits much slower outside the source regions after being lifted into the free troposphere, e.g., longer than 10 days over the subtropical oceans and in the high latitudes. In comparison, it is less than 1-2 days over the source regions or in the tropical precipitating regions and mid-latitude frontal systems where wet removal is efficient. Refining the horizonal grid spacing may lead to shorter dust lifetime, because of the higher surface windspeed that increases friction velocity, thus causing larger dry deposition velocity at the surface (L. Zhang et al., 2001). In addition, dust dry deposition rate in the column also depends on the vertical transport of dust particles, which is enhanced within HRes (discussed below in Section 4.2). Since the free-troposphere dust is removed by sedimentation only, slower than the boundary-layer dust, the enhanced vertical transport will thus lead to longer dust lifetime. This effect generally dominates the increased surface dry deposition velocity over the convective dust source regions, resulting in longer dust lifetime in those regions (Fig. 7f), such as in North Africa for more than 0.5 day (~+50%). On the other hand, dust wet deposition is enhanced in HRes due to resolved cloud and precipitation fields, decreasing the local lifetime of the transported dust, e.g., over the subtropical southeasten Atlantic and northeastern Pacific. Longer (shorter) dust lifetime contributes to a larger (smaller) dust burden, therefore, enhanced (reduced) DAOD in those regions, but also the net changes in DAOD also depend on the modified emissions that determine the amount of dust mobilized and emitted to the atmosphere.

Opposing to the effect of the horizontal refinement (Fig. 7b), increasing the number of vertical layers from 30 in LResZ30 to 72 in LRes leads to the reduction of DAOD over most of

the dust-influenced regions as shown in Fig. 8a, except for a few downwind regions. These changes in DAOD also cannot be explained solely by the emission changes in Fig. 8b, as LRes with finer vertical resolution produces different profiles of stability and turbulence, which in fact causes higher surface winds, thus stronger dust mobilization over most of the erodible surfaces, e.g., the western North Africa, where the DAOD changes, however, are primarily negative. As discussed above, the higher surface winds in LRes also enhance the surface deposition velocity, thus reducing the residence time of dust over the source regions (Fig. 8c). Therefore, LRes predicts less elevated dust to the free troposphere and advected in long distances than LResZ30 (discussed below in Section 4.3), thus smaller DAODs near the source regions, e.g., for the North African dust plumes over the equatorial Atlantic Ocean and South America. The weakened wet removal in LRes relative to LResZ30 increases the local lifetime of the transported dust over most of the remote oceans, which may or may not lead to larger DAOD values depending also on the changes of local dust burden from transport.

It is worth noting that the ambient atmospheric conditions especially relative humidity, to which DAOD is sensitive, could also be influenced by the resolution changes (both horizontally and vertically) through the dust climate feedback in the free-running model simulations. It is considered to be secondary though, compared to the direct changes in dust aerosol fields discussed here.

4.3 Effects of Increasing Resolution on Vertical Distribution

In addition to the column integrated DAOD, dust vertical distribution is also sensitive to the model resolution as shown in Figure 9. LRes predicts the weakest vertical transport of dust around the major dust sources in both hemispheres, i.e., 15°N, followed by 40°N and 25°S, consistent with the shortest dust lifetime (Table 4). Compared to LRes, both HRes (with higher horizontal resolution) and LResZ30 (with lower vertical resolution) simulate enhanced uplift of dust to the upper troposphere, leading to greater global burdens. Thus, model refinement in the horizontal (from LRes to HRes) has the opposing effects on dust vertical distribution compared to refining the vertical resolution (from LResZ30 to LRes). The main difference between them is that the vertical transport of dust in HRes with increased horizontal resolution is enhanced, as a result of resolved convective or nonconvective (e.g., orographic) ascent and stronger turbulent mixing in the boundary layer (indicated by a smaller contribution from the turbulent deposition in dry

654 removal), while a weaker upward transport of dust is simulated by LRes with increased vertical
655 resolution, because of the enhanced dust dry deposition at the surface associated with stronger
656 surface winds. Although HRes also predicts higher surface winds thus larger surface deposition,
657 this effect on dust vertical distribution is weaker over the source regions thus dominated by the
658 enhancement of vertical motion that enables stronger vertical transport of dust particles in HRes.
659 The strong sensitivity of dust vertical distribution to the varying model resolution through
660 interactions with surface winds and boundary-layer dynamics cleary demonstrates that the model
661 representations of the surface dry deposition, sedimentation and vertical transport processes of
662 dust are highly scale-dependent, besides the dust emission parameterization.

663 While LResZ30 does not change the zonal-mean maximum dust source locations from
664 LRes, i.e., still center around the 15°N latitudes, HRes shows the increased relative strength of
665 dust loadings around 40°N as well as 30°N and 25°S, because the emissions in those regions have
666 a stronger dependency on resolved surface winds than those areas near 15°N. The enhanced dust
667 vertical transport around 40°N in HRes further leads to the stronger poleward transport in the upper
668 troposphere above 500 hPa. Because of the low mass extinction coefficient and low hygroscopicity
669 of dust aerosols especially in the free troposphere, these model discrepancies in dust vertical
670 mixing ratios do not make substantial differences in DAOD, e.g., in the high latitudes (<0.01, Fig.
671 7b). Therefore, the dust vertical distribution is not well constrained by the column integrated
672 DAOD, in particular the global mean DAOD. The elevated dust, on the other hand, could act as
673 highly-active ice nucleation particles in mixed or ice phase clouds causing changes to indirect
674 radiative effects. It is critical to constrain the vertical transport of dust into the free troposphere.

675 **4.4 Effects of Increasing Resolution on Deposition Fluxes**

676 As a key input to the ocean biogeochemistry, it is important to examine the sensitivity of
677 the absolute dust depositon fluxes to model resolution in line with the development of the high-
678 resolution coupled ESMs. The differences in the simulated dust deposition fluxes between
679 different resolution configurations are shown in Fig. 10. Since the dust deposition fluxes
680 corresponds to the emissions, HRes simulates larger deposition fluxes than LRes over most of the
681 domain, except for the areas influenced by the lowered emissions or with enhanced removal. In
682 particular, over the major high-nutrient low-chlorophyll biological regions in the sub-Arctic
683 Pacific and Southern Ocean, dust deposition fluxes are increased by >25% in HRes, suggesting an

enhanced nutrient supply to the ocean biogeochemistry if coupled with a higher-resolution atmospheric model. Additionally, the HRes model also predicts more than 2-fold annual dust deposition into the Arctic region than LRes, which could have important implications on the acceleration of ice/snow melting in the high latitudes by lowering the surface albedo. In contrast, the impact of higher vertical resolution is opposing to the horizonal refinement. Compared to LResZ30, LRes predicts larger deposition fluxes over the major dust sources including Antarctic (Fig. 8c), but underestimes in most of the other regions, except for a few regions with higher DAOD (thus larger burden) due to increased lifetime (Fig. 8c). These differences in the changes of dust deposition fluxes with higher horizontal or vertical resolution correspond largely to the DAOD changes (dust burden changes), which in turn depend on the combined effects on various dust processes discussed in Section 4.2.

Compared with the observational data in Fig. 6c and Table 3, the model underestimation in the remote oceans such as N. Pacific is reduced with HRes, since it predicts larger deposition fluxes than LRes over most of the domain. But the overestimation in the absolute dust deposition fluxes over the dust-laden regions such as N. Africa and the adjacent subtropical Atlantic is enlarged by HRes, except for Antarctic, where the model high bias is substantially reduced (i.e., by a factor of 4 in the Table 3) due to the lowered Antarctic dust emissions (Fig. 7d). Contrary to the HRes-induced changes, the LRes simulations of dust deposition agree better with the observations than LResZ30 over the main dust deposition oceans near the sources but are even more underestimated in the remote oceans. As shown in the Table 3 and Fig. 6c, the resolution effects on deposition fluxes have a larger impact in the remote regions, whereas near the sources, dust deposition fluxes are influenced more by the model representation of dust properties, e.g., particle size, sphericity, or deposition velocity, which either the low or high resolution E3SMv1 simulations are high-biased.

4.5 Dust Direct Radiative Effects

Figure 11 shows the calculated DRE of dust at TOA with the different E3SMv1 configurations. LRes, which is the default E3SMv1 configuration, predicts positive DREs of dust over the major source regions such as Sahara, Arabian Peninsula and Central Asia, exceeding 10 Wm^{-2}, due to the light absorption of dust minerals when located over the highly reflective surfaces. Also, moderately positive DREs of dust are estimated over the mid-latitude oceans likely above

the storm tracks and snow- or ice-covered surface in high latitudes, while negative DREs are found in the lower latitudes over oceans or land associated with relatively dark surfaces. Overall, the mean dust DRE by LRes gives a slightly negative global forcing of -0.08 Wm^{-2} at TOA. Using the less-absorbing imaginary indices inferred from the AERONET measurements, LResT predicts more negative DREs over most of the domain, mainly because of the reduced dust SW absorption (AAOD). The globally averaged net DRE of dust decreases to -0.42 Wm^{-2}, which is more negative about a factor of five higher in magnitude than LRes. The model-calculated global energy budgets in the column: at the TOA, in the atmosphere and at surface, are summarized in Table 5. About 2/3 of the reduction in the TOA DRE estimated by LResT relative to LRes is due to the lower atmospheric absorption in SW (about 50% less), which is consistent with the AAOD reduction (Section 3.1). Additionally, LResT also predicts more boundary-layer dusts and less vertical and horizontal transport than LRes in comparison with CALIPSO (Section 3.2), which further contributes to the more negative DREs in SW, as the boundary-layer dusts are less likely to be lifted above the clouds with a brigher underlying surface. For the LW DRE, LResT increases slightly from +0.08 Wm^{-2} in LRes to 0.1 Wm^{-2}, as shown in Table 5, due to the increased LW warming of coarse-mode dust (Kok et al., 2017). Therefore, the net DRE differences between LResT and LRes are primarily attributable to the SW DRE changes.

The impact of increasing horizontal resolution on dust DRE is illustrated in Figure 11c for differences between HResT and LResT_HRtuned (same as LResT but using the high-resolution tuning parameters). Therefore, differences in the estimated dust DRE between HResT and LResT_HRtuned are attributable to the resolution effect on dust simulations solely, i.e., not affected by the different physics tuning parameters. Both simulations are performed with the updated dust size distribution and optical properties as in LResT that are planned for the next version of E3SM, i.e., E3SMv2. They are also tuned to the same global DAOD of about 0.038~0.04, which is slightly higher than LResT (in order to get a HResT AOD close to the satellite estimate of 0.14) but still within the uncertainty of the observational estimate (0.03±0.01). As shown in Fig. 11c, higher horizontal resolution leads to regionally dependent changes in the predicted dust DREs. The geographical pattern of the DRE differences between HResT and LResT_HRtuned corresponds approximately to the DAOD changes between HRes and LRes in Fig. 7b. Specifically, higher DAODs with the finer-resolution simulations (HResT or HRes) result in stronger dust DREs, either more positively or negatively, relative to the coarse-resolution

simulations (LResT or LRes). For instance, the strength of the positive DREs of dust over the Sahara Desert and Arabian Peninsula would be enhanced by increasing horizontal resolution, as well as the negative effects in most of the Asia (Fig. 7b). On the other hand, because of the decreased DAODs, the negative DREs of dust downwind of the North African sources across the Atlantic Ocean and over the South America would be weakened with higher resolution. In addition to DAOD, the resolution effect on dust vertical distribution also affects the strength of dust DREs. More dusts particles can loft at the higher resolution, leading to the weakening (positive changes) of the negative DREs over Central Asia (Fig. 9b), despite the increased DAOD. Since the LW DRE of dust increases with height, it is enhanced globally by +0.02 Wm^{-2} (14%) in HResT (Table 5), comparable to the effect of changing the dust size distribution. The impact of increasing resolution on the globally averaged dust net DRE is small with a slightly weaker negative effect due to the enhanced LW warming, although the regional changes are greater and different in sign.

The comparison of the estimated dust DREs with other modeling studies is shown in Figure 12 for the SW, LW and net effects, respectively. In order to reduce the influences from different DAODs, the DRE estimates from HResT are scaled to a global DAOD of 0.029 same as the E3SM low resolution runs (LRes and LResT), and denoted as HResT* in Fig. 12 and Table 5. The default E3SMv1 model (LRes) predicts a small dust net DRE with a negative value of -0.08 Wm^{-2} at TOA, which is more positive than -0.17 Wm^{-2} from CAM5 (Scanza et al., 2015), -0.45 Wm^{-2} by the AeroCom models taken from Kok et al. (2017) and an observationally constrained estimate of -0.2 Wm^{-2} (Kok et al., 2017), primarily due to the weaker SW cooling (smaller negative SW DRE). After updating the dust SW absorption and size-segregated emissions, E3SMv1 at both low and high resolutions (LResT and HResT*) estimates a more negative net DRE of about -0.42 Wm^{-2}, which is within the AeroCom model estimates (-0.3 to -0.6 Wm^{-2}), although both the SW and LW effects are relatively lower. Kok et al. (2017) suggested that the fine-size bias in the AeroCom models probably contributed to their larger SW cooling. Indeed, the updated E3SM with the size correction that shifts more emitted dust particles from the accumulation mode toward larger sizes (diameter$\leq$10μm) predicts a SW DRE of ~-0.5 Wm^{-2}, and agrees better with CAM5 (Scanza et al., 2015) and the observationally constrained estimate (Kok et al., 2017). Kok et al. (2017) also includes coarser particles with 10μm$\leq$diameter$\leq$20μm and a recent study by Di Biagio et al. (2020) shows that even coarser particles with diameter$\geq$20μm should be considered in global models. These very coarse particles would further reduce the contribution by smaller (cooling)

776 particles to the global dust cycle, as Di Biagio et al. (2020) obtains a smaller negative DRE in SW
777 (-0.25 Wm^{-2}), about half of the other model calculations.

778 Dust particle size is also one of the large sources of uncertainty for the LW effect. The size
779 correction implemented to E3SM and higher horizontal resolution increases the LW warming
780 effect by 50% from +0.08 to +0.01 and +0.12 Wm^{-2} progressively, but it is still lower than other
781 studies ranging from +0.17 to +0.25 Wm^{-2} as shown in Fig. 12. Inclusion of the coarser particles
782 (diameter≥10μm) to E3SMv1 would directly increase the estimated dust LW effect, e.g., Kok et
783 al. (2017) indicates that the coarse dust particles (i.e., 10μm≤diameter≤20μm) could produce an
784 additional positive DRE of 0.03 Wm^{-2} (0.01 to 0.06) globally. The uncertainty in LW DRE may
785 also stem from the dust refractive indices, as E3SMv1 neglects the regional variability in dust LW
786 optics (Di Biagio et al., 2017), e.g., which changes their DRE LW estimates between +0.09 and
787 +0.36 Wm^{-2}. Another uncertainty is from the LW scattering that is not considered in E3SMv1 but
788 by other studies such as Kok et al. (2017). In addition, the LW effect is very sensitive to the dust
789 layer height, which is one of the least constrained dust properties in models compared with the
790 observations, and could potentially cause great inter-modal differences. As discussed in Section
791 4.3, the higher horizontal and vertical resolution of E3SMv1 have a large impact on the dust
792 vertical distribution that may contribute to the differences in LW DRE.

793 To exclude the uncertainty in DAOD, the DRE efficiency, defined as the DRE produced
794 per unit of global DAOD, is calculated. For E3SMv1, it ranges from 3.5 (LResT) to 4 Wm^{-2}
795 (HResT) in LW, both of which are lower than those of CAM5 (5.2 Wm^{-2}) and the observational
796 estimate (8.3 Wm^{-2}). For the SW DRE efficiency, E3SMv1 generates the largest negative values
797 from -17.9 (LResT) to -18.3 Wm^{-2} (HResT) compared to the -10. Wm^{-2} by CAM5 and -16.7 Wm^{-2}
798 constrained by the observations. Similar to the direct comparison of DRE, the consistently low
799 (or high) differences in LW (or SW) DRE efficiencies estimated by E3SMv1 indicate that the
800 globally averaged dust size in this global model might still be too small assuming the
801 observationally constrained estimates provide the correct ranges with high-quality datasets.
802 Including coarser dust particles would generate larger LW warming and smaller SW cooling that

803 could nudge the calculated DRE efficiencies toward the observational estimates. Other
804 uncertainties as mentioned above might also help to explain the differences.

805 **5. Discussion and Conclusions**

806 Quantification of dust life cycle and radiative effects in ESMs has important implications
807 for improving the model's capabilities for water cycle and biogeochemistry studies in response to
808 climate change. Unlike anthropogenic aerosols, dust aerosols not only influence the climate system
809 as an external forcer but also account for a significant fraction of the direct climate feedback
810 associated with all aerosols (Kok et al., 2018). Because the dust simulation is sensitive to the model
811 representation of meteorological and climate states, dust simulations are often subject to great
812 uncertainties, as indicated by a wide diversity in simulated dust quantities among models and
813 between models and observations (Huneeus et al., 2011; A. Zhao et al., 2021). These uncertainties,
814 most of which are unconstrained, further affect the assessment of dust radiative and climate effects.
815 As part of development of the DOE E3SM on exascale computing platforms, this study examines
816 the simulated global life cycle and direct radiative effects of dust in the recently released E3SMv1,
817 resulting from model physics improvements and increased model resolution.

818 Our study shows that the default E3SMv1 constrained by the global DAOD simulates the
819 geographical pattern and seasonal variations in DAOD reasonably well, compared with the
820 AERONET surface measurements. On the other hand, it overestimates the dust aerosol absorption
821 in SW by a factor of two, which leads to a more positive net DRE (-0.08 Wm^{-2}) than its precedent
822 model CAM5 (-0.17 Wm^{-2}). By switching to the less absorbing dust refractive indices as well as
823 an emission size distribution with more coarse particles emitted, the dust SW cooling simulated
824 by E3SMv1 is increased and is closer to the observationally based estimate by Kok et al. (2017).
825 For dust vertical distribution, E3SMv1 captures seasonal variations of the elevated dust layers over
826 the major source regions, but underpredicts the dust extinctions compared with the CALIOP data,
827 especially in the upper troposphere. The low biases in the model simulations are greater in summer
828 than winter. As a result of the underestimation of vertical transport, E3SMv1 also predicts a weaker
829 long-range transport of dust compared with the satellite observations and a shorter dust lifetime
830 (~2 days) than most of other models. The simulated deposition fluxes are underestimated in remote

oceans, but the global dust deposition is dominated by the high biases near the sources over the main dust deposition regions, compared with the climatology data composite.

The impact of increasing model resolution on dust simulations was examined with E3SMv1. It is critical to understand what individual dust processes are scale- or resolution-dependent and the subsequent impact on the dust radiative effects and deposition fluxes for implications on future development of high-resolution ESMs such as the Simple Cloud-Resolving E3SM Atmospheric Model (SCREAM) (Caldwell et al., 2021) or regionally refined variable resolution ESMs (Tang et al., 2019). This study finds that in addition to the emission fluxes, dust removal, especially dry deposition rate, is highly scale-dependent, which in turn affects the dust lifetime, atmospheric burden and DAOD. Specifically, increasing horizontal resolution (from 100km to 25km) without tuning results in a larger enhancement in global DAOD (+42%) than seen in the emissions themselves (+29%), because it is combined with a reduction of dry deposition rate (-21%) and increase of lifetime. With the global tuning of DAOD (through dust emissions), it still leads to a decreased dry deposition rate by -17%. In contrast, refinement of vertical resolution (from 30 to 72 layers) increases the dust dry deposition rate (+45%), thus resulting in a shorter lifetime, opposing to the horizontal effect. The global wet removal of dust is relatively less sensitive to the increased model resolution both horizontally and vertically.

Futhermore, we showed that the uniform scaling of dust emission factor to constrain global DAOD does not eliminate the remarkable and nonuniform changes of DAOD on the regional scales, due to the compound resolution effects on dust emissions, removal, and vertical transport. Dust vertical distribtuions and deposition fluxes are also highly sensitive to the resolution changes, and these quantities are not well constrained by the column integrated DAOD, in particular the global mean. As the elevated dusts in the free troposphere are a major source of ice nucleation particles for mixed- and ice- phase clouds and the nutrient-enriching dust deposition is vital for terrestrial and ocean ecosystems, better observational constraints of dust vertical distribution and deposition fluxes are needed for representing the dust indirect radiative and biogeochemical effects in the future ESMs with higher resolution.

The global DAOD constraint does effectively curb the impact of increasing horizontal resolution on the global mean dust net DRE. Compared to the low-resolution configuration of E3SMv1, the high-resolution configuration by 4 times in the horizontal estimates a slightly weaker

negative dust DRE by about 4% (+0.03 Wm^{-2}). However, the large regional differences in DAOD and vertical distributions with higher model resolution can lead to positive or negative direct perburbations on the energy balance ranging from -9 to +4 Wm^{-2} on the annual mean basis, which is sufficient to potentially affect the regional hydrological cycle. The updated dust optics and emission size distribution lead to improved dust SW and net DREs of -0.52 Wm^{-2} and -0.42 Wm^{-2} than the default E3SMv1, compared with the observationally based estimates of -0.5 (-0.85 to -0.15 Wm^{-2}) and -0.2 (-0.48 to +0.2 Wm^{-2}). But even with the corrected fine-size bias in dust particles upon emission, the calculated SW and LW DRE efficiencies by E3SM still indicate that the globally averaged dust size might still be too small, compared with the observations, showing a stronger SW cooling and weaker LW warming. This finding about the atmospheric presence of possibly more coarser dust particles is consistent with some recent global model studies (Di Biagio et al., 2020; Kok et al., 2017). Other uncertainties such as the dust LW scattering (Dufresne et al., 2002), refractive indices (Di Biagio et al., 2017), mineral speciation (Li et al., 2021), and particle sphericity (Hamilton et al., 2020) could also contribute to the inter-modal differences in dust DRE.

It is challenging to constrain the simulated dust life cycle with multiple observational variables, amid uncertainties in the datasets. In E3SMv1, the evaluation of dust DRE suggests that the abundance of coarse particles may be underrepresented in all model configuration, but simply shifting particles upon emission or in transport toward large sizes would aggravate the high biases in the simulated dust deposition fluxes near the sources and low biases in remote oceans. To harmonize these uncertainties, further investigation into constraining processes affecting long range transport and improving dust dry deposition and convective transport to the upper atmosphere is warranted. Furthermore, this study demonstrates the strong sensitivity of model representation of dust processes beyond emissions (such as dry deposition and vertical transport) to both horizontal and vertical model resolution, and the impact on direct radiative effects of dust. It also adds a cautionary note to the use of global dust AOD at 550nm as the only constraint for

886 dust simulations, highlighting the need of developing observational constraints for dust size, LW
887 optical properties and vertical profiles as well as variability in deposition fluxes.

888

889 **Acknowledgments**

890 This research was supported as part of the Energy Exascale Earth System Model (E3SM) project,
891 funded by the U.S. Department of Energy (DOE), Office of Science, Office of Biological and
892 Environmental Research (BER). The authors thank all the E3SM project team members for their
893 efforts in developing and supporting the E3SM. YF would like to to acknowledge the support of
894 Argonne National Laboratory (ANL) provided by the U.S. DOE Office of Science, under
895 Contract No. DE-AC02-06CH11357. The Pacific Northwest National Laboratory (PNNL) is
896 operated for U.S. DOE by Battelle Memorial Institute under contract DE-AC05-76RL01830. The
897 work at Lawrence Livermore National Laboratory (LLNL) was performed under the auspices of
898 the U.S. DOE by Lawrence Livermore National Laboratory under Contract DE-AC52-
899 07NA27344. The work at Brookhaven National Laboratory (BNL) was supported by the U.S.
900 DOE Office of Science under contract DE-SC0012704. DSH and NMM would like to
901 acknowledge support from DOE DE-SC0021302. HY was supported by NASA
902 CALIPSO/CloudSat Science Team project administered by David Considine. Simulations and
903 analysis were performed by using the computing cluster (Anvil) supported by the BER Earth
904 System Modeling program and operated by the Laboratory Computing Resource Center (LCRC)
905 at ANL, as well as the computational resources at the National Energy Research Scientific
906 Computing Center (NERSC), a DOE Office of Science User Facility supported by the Office of
907 Science of the U.S. Department of Energy under contract DE-AC02-05CH11231.

908 **Code and Data Availability**

909 The E3SM project, code, simulation configurations, model output, and tools to work with the
910 output are described at the website (https://e3sm.org). The E3SMv1 model has been released and
911 made available through the GitHub repository (https://github.com/E3SM-Project/E3SM). Model
912 output data are accessible directly on NERSC.

913

914 **References**

915

916 Adebiyi, A. A., & Kok, J. F. (2020). Climate models miss most of the coarse dust in the atmosphere. *Science*
917 *Advances, 6*(15), eaaz9507. https://www.science.org/doi/abs/10.1126/sciadv.aaz9507
918 Albani, S., Mahowald, N. M., Perry, A. T., Scanza, R. A., Zender, C. S., Heavens, N. G., et al. (2014). Improved
919 dust representation in the Community Atmosphere Model. *Journal of Advances in Modeling Earth Systems,*
920 *6*(3), 541-570. <Go to ISI>://WOS:000344387900004
921 Amiri-Farahani, A., Allen, R. J., Neubauer, D., & Lohmann, U. (2017). Impact of Saharan dust on North Atlantic
922 marine stratocumulus clouds: importance of the semidirect effect. *Atmospheric Chemistry and Physics,*
923 *17*(10), 6305-6322. <Go to ISI>://WOS:000401923600001
924 Caldwell, P. M., Mametjanov, A., Tang, Q., Van Roekel, L. P., Golaz, J. C., Lin, W. Y., et al. (2019). The DOE
925 E3SM Coupled Model Version 1: Description and Results at High Resolution. *Journal of Advances in*
926 *Modeling Earth Systems*. <Go to ISI>://WOS:000502308300001

927 Caldwell, P. M., Terai, C. R., Hillman, B., Keen, N. D., Bogenschutz, P., Lin, W., et al. (2021). Convection-
928 Permitting Simulations with the E3SM Global Atmosphere Model. *Journal of Advances in Modeling Earth*
929 *Systems, n/a*(n/a), e2021MS002544. https://doi.org/10.1029/2021MS002544.
930 https://doi.org/10.1029/2021MS002544
931 Choobari, O. A., Zawar-Reza, P., & Sturman, A. (2014). The global distribution of mineral dust and its impacts on
932 the climate system: A review. *Atmospheric Research, 138*, 152-165. <Go to
933 ISI>://WOS:000333504300012
934 DeMott, P. J., Prenni, A. J., Liu, X., Kreidenweis, S. M., Petters, M. D., Twohy, C. H., et al. (2010). Predicting
935 global atmospheric ice nuclei distributions and their impacts on climate. *Proceedings of the National*
936 *Academy of Sciences of the United States of America, 107*(25), 11217-11222. <Go to
937 ISI>://WOS:000279058000014
938 DeMott, P. J., Prenni, A. J., McMeeking, G. R., Sullivan, R. C., Petters, M. D., Tobo, Y., et al. (2015). Integrating
939 laboratory and field data to quantify the immersion freezing ice nucleation activity of mineral dust
940 particles. *Atmospheric Chemistry and Physics, 15*(1), 393-409. <Go to ISI>://WOS:000347958200023
941 DeMott, P. J., Sassen, K., Poellot, M. R., Baumgardner, D., Rogers, D. C., Brooks, S. D., et al. (2003). African dust
942 aerosols as atmospheric ice nuclei. *Geophysical Research Letters, 30*(14). <Go to
943 ISI>://WOS:000184599400002
944 Dentener, F. J., Carmichael, G. R., Zhang, Y., Lelieveld, J., & Crutzen, P. J. (1996). Role of mineral aerosol as a
945 reactive surface in the global troposphere. *Journal of Geophysical Research-Atmospheres, 101*(D17),
946 22869-22889. <Go to ISI>://WOS:A1996VN18400012
947 Di Biagio, C., Balkanski, Y., Albani, S., Boucher, O., & Formenti, P. (2020). Direct Radiative Effect by Mineral
948 Dust Aerosols Constrained by New Microphysical and Spectral Optical Data. *Geophysical Research*
949 *Letters, 47*(2), e2019GL086186. https://agupubs.onlinelibrary.wiley.com/doi/abs/10.1029/2019GL086186
950 Di Biagio, C., Formenti, P., Balkanski, Y., Caponi, L., Cazaunau, M., Pangui, E., et al. (2017). Global scale
951 variability of the mineral dust long-wave refractive index: a new dataset of in situ measurements for
952 climate modeling and remote sensing. *Atmos. Chem. Phys., 17*(3), 1901-1929.
953 https://acp.copernicus.org/articles/17/1901/2017/
954 Does, M. v. d., Knippertz, P., Zschenderlein, P., Harrison, R. G., & Stuut, J.-B. W. (2018). The mysterious long-
955 range transport of giant mineral dust particles. *Science Advances, 4*(12), eaau2768.
956 https://www.science.org/doi/abs/10.1126/sciadv.aau2768
957 Doherty, O. M., & Evan, A. T. (2014). Identification of a new dust-stratocumulus indirect effect over the tropical
958 North Atlantic. *Geophysical Research Letters, 41*(19), 6935-6942. <Go to ISI>://WOS:000344913800052
959 Dubovik, O., & King, M. D. (2000). A flexible inversion algorithm for retrieval of aerosol optical properties from
960 Sun and sky radiance measurements. *Journal of Geophysical Research-Atmospheres, 105*(D16), 20673-
961 20696. <Go to ISI>://WOS:000089107600017
962 Dubovik, O., Smirnov, A., Holben, B. N., King, M. D., Kaufman, Y. J., Eck, T. F., & Slutsker, I. (2000). Accuracy
963 assessments of aerosol optical properties retrieved from Aerosol Robotic Network (AERONET) Sun and
964 sky radiance measurements. *Journal of Geophysical Research-Atmospheres, 105*(D8), 9791-9806. <Go to
965 ISI>://WOS:000086658600004
966 Dufresne, J. L., Gautier, C., Ricchiazzi, P., & Fouquart, Y. (2002). Longwave scattering effects of mineral aerosols.
967 *Journal of the Atmospheric Sciences, 59*(12), 1959-1966. <Go to ISI>://WOS:000175533700003
968 Eastham, S. D., & Jacob, D. J. (2017). Limits on the ability of global Eulerian models to resolve intercontinental
969 transport of chemical plumes. *Atmospheric Chemistry and Physics, 17*(4), 2543-2553. <Go to
970 ISI>://WOS:000395136300001
971 Emerson, E. W., Hodshire, A. L., DeBolt, H. M., Bilsback, K. R., Pierce, J. R., McMeeking, G. R., & Farmer, D. K.
972 (2020). Revisiting particle dry deposition and its role in radiative effect estimates. *Proceedings of the*
973 *National Academy of Sciences, 117*(42), 26076. http://www.pnas.org/content/117/42/26076.abstract
974 Evan, A. T., Flamant, C., Fiedler, S., & Doherty, O. (2014). An analysis of aeolian dust in climate models.
975 *Geophysical Research Letters, 41*(16), 5996-6001. <Go to ISI>://WOS:000342755400040
976 Evan, A. T., Foltz, G. R., Zhang, D. X., & Vimont, D. J. (2011). Influence of African dust on ocean-atmosphere
977 variability in the tropical Atlantic. *Nature Geoscience, 4*(11), 762-765. <Go to
978 ISI>://WOS:000296723500013
979 Fan, Leung, L. R., DeMott, P. J., Comstock, J. M., Singh, B., Rosenfeld, D., et al. (2014). Aerosol impacts on
980 California winter clouds and precipitation during CalWater 2011: local pollution versus long-range
981 transported dust. *Atmos. Chem. Phys., 14*(1), 81-101. https://www.atmos-chem-phys.net/14/81/2014/

Feng, Y., & Penner, J. E. (2007). Global modeling of nitrate and ammonium: Interaction of aerosols and tropospheric chemistry. *Journal of Geophysical Research-Atmospheres, 112*(D1). <Go to ISI>://WOS:000243352300001

Forster, P., Ramaswamy, V., Artaxo, P., Berntsen, T., Betts, R., Fahey, D. W., et al. (2007). Changes in Atmospheric Constituents and in Radiative Forcing. In *Climate Change 2007: The Physical Science Basis. Contribution of Working Groups I to the Fourth Assessment Report of the Intergovernmental Panel on Climate Change*. Cambridge, United Kingdom and New York, NY, USA: Cambridge University Press.

Ghan, S. J., Liu, X., Easter, R. C., Zaveri, R., Rasch, P. J., Yoon, J. H., & Eaton, B. (2012). Toward a Minimal Representation of Aerosols in Climate Models: Comparative Decomposition of Aerosol Direct, Semidirect, and Indirect Radiative Forcing. *Journal of Climate, 25*(19), 6461-6476. <Go to ISI>://WOS:000309653800001

Ghan, S. J., & Zaveri, R. A. (2007). Parameterization of optical properties for hydrated internally mixed aerosol. *Journal of Geophysical Research-Atmospheres, 112*(D10). <Go to ISI>://WOS:000246838800003

Golaz, J. C., Caldwell, P. M., Van Roekel, L. P., Petersen, M. R., Tang, Q., Wolfe, J. D., et al. (2019). The DOE E3SM Coupled Model Version 1: Overview and Evaluation at Standard Resolution. *Journal of Advances in Modeling Earth Systems, 11*(7), 2089-2129. <Go to ISI>://WOS:000480282800012

Hamilton, D. S., Perron, M. M. G., Bond, T. C., Bowie, A. R., Buchholz, R. R., Guieu, C., et al. (2022). Earth, Wind, Fire, and Pollution: Aerosol Nutrient Sources and Impacts on Ocean Biogeochemistry. *Annual Review of Marine Science, 14*(1), null. https://www.annualreviews.org/doi/abs/10.1146/annurev-marine-031921-013612

Hamilton, D. S., Scanza, R. A., Feng, Y., Guinness, J., Kok, J. F., Li, L. L., et al. (2019). Improved methodologies for Earth system modelling of atmospheric soluble iron and observation comparisons using the Mechanism of Intermediate complexity for Modelling Iron (MIMI v1.0). *Geoscientific Model Development, 12*(9), 3835-3862. <Go to ISI>://WOS:000484142100001

Hamilton, D. S., Scanza, R. A., Rathod, S. D., Bond, T. C., Kok, J. F., Li, L., et al. (2020). Recent (1980 to 2015) Trends and Variability in Daily-to-Interannual Soluble Iron Deposition from Dust, Fire, and Anthropogenic Sources. *Geophysical Research Letters, 47*(17), e2020GL089688. https://agupubs.onlinelibrary.wiley.com/doi/abs/10.1029/2020GL089688

Hess, M., Koepke, P., & Schult, I. (1998). Optical properties of aerosols and clouds: The software package OPAC. *Bulletin of the American Meteorological Society, 79*(5), 831-844. <Go to ISI>://WOS:000073809200007

Huneeus, N., Schulz, M., Balkanski, Y., Griesfeller, J., Prospero, J., Kinne, S., et al. (2011). Global dust model intercomparison in AeroCom phase I. *Atmospheric Chemistry and Physics, 11*(15), 7781-7816. <Go to ISI>://WOS:000293826500024

Iacono, M. J., Delamere, J. S., Mlawer, E. J., Shephard, M. W., Clough, S. A., & Collins, W. D. (2008). Radiative forcing by long-lived greenhouse gases: Calculations with the AER radiative transfer models. *Journal of Geophysical Research-Atmospheres, 113*(D13). <Go to ISI>://WOS:000257431600004

Jickells, T. D., An, Z. S., Andersen, K. K., Baker, A. R., Bergametti, G., Brooks, N., et al. (2005). Global iron connections between desert dust, ocean biogeochemistry, and climate. *Science, 308*(5718), 67-71. <Go to ISI>://WOS:000228221500033

Kim, D., Chin, M., Yu, H. B., Diehl, T., Tan, Q., Kahn, R. A., et al. (2014). Sources, sinks, and transatlantic transport of North African dust aerosol: A multimodel analysis and comparison with remote sensing data. *Journal of Geophysical Research-Atmospheres, 119*(10), 6259-6277. <Go to ISI>://WOS:000337766600034

Kok, J. F. (2011). Does the size distribution of mineral dust aerosols depend on the wind speed at emission? *Atmospheric Chemistry and Physics, 11*(19), 10149-10156. <Go to ISI>://WOS:000296357300009

Kok, J. F., Adebiyi, A. A., Albani, S., Balkanski, Y., Checa-Garcia, R., Chin, M., et al. (2021). Improved representation of the global dust cycle using observational constraints on dust properties and abundance. *Atmos. Chem. Phys., 21*(10), 8127-8167. https://acp.copernicus.org/articles/21/8127/2021/

Kok, J. F., Mahowald, N. M., Fratini, G., Gillies, J. A., Ishizuka, M., Leys, J. F., et al. (2014). An improved dust emission model - Part 1: Model description and comparison against measurements. *Atmospheric Chemistry and Physics, 14*(23), 13023-13041. <Go to ISI>://WOS:000346140100026

Kok, J. F., Ridley, D. A., Zhou, Q., Miller, R. L., Zhao, C., Heald, C. L., et al. (2017). Smaller desert dust cooling effect estimated from analysis of dust size and abundance. *Nature Geoscience, 10*(4), 274-278. <Go to ISI>://WOS:000398162800014

Kok, J. F., Ward, D. S., Mahowald, N. M., & Evan, A. T. (2018). Global and regional importance of the direct dust-climate feedback. *Nature Communications, 9*. <Go to ISI>://WOS:000422649500003

Lau, K. M., Kim, K. M., Sud, Y. C., & Walker, G. K. (2009). A GCM study of the response of the atmospheric water cycle of West Africa and the Atlantic to Saharan dust radiative forcing. *Annales Geophysicae, 27*(10), 4023-4037. <Go to ISI>://WOS:000271356500028

Li, L., Mahowald, N. M., Miller, R. L., Pérez García-Pando, C., Klose, M., Hamilton, D. S., et al. (2021). Quantifying the range of the dust direct radiative effect due to source mineralogy uncertainty. *Atmos. Chem. Phys., 21*(5), 3973-4005. https://acp.copernicus.org/articles/21/3973/2021/

Liu, Easter, R. C., Ghan, S. J., Zaveri, R., Rasch, P., Shi, X., et al. (2012). Toward a minimal representation of aerosols in climate models: description and evaluation in the Community Atmosphere Model CAM5. *Geoscientific Model Development, 5*(3), 709-739. <Go to ISI>://WOS:000305964700001

Liu, Ma, P. L., Wang, H., Tilmes, S., Singh, B., Easter, R. C., et al. (2016). Description and evaluation of a new four-mode version of the Modal Aerosol Module (MAM4) within version 5.3 of the Community Atmosphere Model. *Geoscientific Model Development, 9*(2), 505-522. <Go to ISI>://WOS:000376933700003

Liu, C., Chu, B., Liu, Y., Ma, Q., Ma, J., He, H., et al. (2013). Effect of mineral dust on secondary organic aerosol yield and aerosol size in α-pinene/NOx photo-oxidation. *Atmospheric Environment, 77*, 781-789. http://www.sciencedirect.com/science/article/pii/S1352231013004378

Lohmann, U., & Diehl, K. (2006). Sensitivity studies of the importance of dust ice nuclei for the indirect aerosol effect on stratiform mixed-phase clouds. *Journal of the Atmospheric Sciences, 63*(3), 968-982. <Go to ISI>://WOS:000236735900010

Ma, P.-L., Rasch, P. J., Wang, M., Wang, H., Ghan, S. J., Easter, R. C., et al. (2015). How does increasing horizontal resolution in a global climate model improve the simulation of aerosol-cloud interactions? *Geophysical Research Letters, 42*(12), 2015GL064183. http://dx.doi.org/10.1002/2015GL064183

Mahowald. (2011). Aerosol Indirect Effect on Biogeochemical Cycles and Climate. *Science, 334*(6057), 794-796. <Go to ISI>://WOS:000296849600043

Mahowald, Engelstaedter, S., Luo, C., Sealy, A., Artaxo, P., Benitez-Nelson, C., et al. (2009). Atmospheric Iron Deposition: Global Distribution, Variability, and Human Perturbations. *Annual Review of Marine Science, 1*, 245-278. <Go to ISI>://WOS:000267421700011

Miller, R. L., Cakmur, R. V., Perlwitz, J., Geogdzhayev, I. V., Ginoux, P., Koch, D., et al. (2006). Mineral dust aerosols in the NASA goddard institute for Space Sciences ModelE atmospheric general circulation model. *Journal of Geophysical Research-Atmospheres, 111*(D6). <Go to ISI>://WOS:000236730400004

Miller, R. L., Tegen, I., & Perlwitz, J. (2004). Surface radiative forcing by soil dust aerosols and the hydrologic cycle. *Journal of Geophysical Research-Atmospheres, 109*(D4). <Go to ISI>://WOS:000189373800006

Myriokefalitakis, S., Ito, A., Kanakidou, M., Nenes, A., Krol, M. C., Mahowald, N. M., et al. (2018). Reviews and syntheses: the GESAMP atmospheric iron deposition model intercomparison study. *Biogeosciences, 15*(21), 6659-6684. https://bg.copernicus.org/articles/15/6659/2018/

Neale, R. B., Chen, C.-C., Gettelman, A., Lauritzen, P. H., Park, S., Williamson, D. L., et al. (2012). Description of the NCAR Community Atmosphere Model (CAM 5.0). *NCAR/TN-486C STR*. http://www.cesm.ucar.edu/models/cesm1.0/cam/docs/description/cam5_desc.pdf

Painter, T. H., Skiles, S. M., Deems, J. S., Bryant, A. C., & Landry, C. C. (2012). Dust radiative forcing in snow of the Upper Colorado River Basin: 1. A 6 year record of energy balance, radiation, and dust concentrations. *Water Resources Research, 48*. <Go to ISI>://WOS:000306905800001

Rasch, P. J., Xie, S., Ma, P. L., Lin, W., Wang, H., Tang, Q., et al. (2019). An Overview of the Atmospheric Component of the Energy Exascale Earth System Model. *Journal of Advances in Modeling Earth Systems, 11*(8), 2377-2411. https://doi.org/10.1029/2019MS001629. https://doi.org/10.1029/2019MS001629

Ridley, D. A., Heald, C. L., Kok, J. F., & Zhao, C. (2016). An observationally constrained estimate of global dust aerosol optical depth. *Atmospheric Chemistry and Physics, 16*(23), 15097-15117. <Go to ISI>://WOS:000389209000005

Ridley, D. A., Heald, C. L., Pierce, J. R., & Evans, M. J. (2013). Toward resolution-independent dust emissions in global models: Impacts on the seasonal and spatial distribution of dust. *Geophysical Research Letters, 40*(11), 2873-2877. <Go to ISI>://WOS:000321261600072

Rosenfeld, D., Rudich, Y., & Lahav, R. (2001). Desert dust suppressing precipitation: A possible desertification feedback loop. *Proceedings of the National Academy of Sciences of the United States of America, 98*(11), 5975-5980. <Go to ISI>://WOS:000168883700010

Scanza, R. A., Mahowald, N., Ghan, S., Zender, C. S., Kok, J. F., Liu, X., et al. (2015). Modeling dust as component minerals in the Community Atmosphere Model: development of framework and impact on radiative forcing. *Atmospheric Chemistry and Physics, 15*(1), 537-561. <Go to ISI>://WOS:000347958200030

Skiles, S. M., Painter, T. H., Deems, J. S., Bryant, A. C., & Landry, C. C. (2012). Dust radiative forcing in snow of the Upper Colorado River Basin: 2. Interannual variability in radiative forcing and snowmelt rates. *Water Resources Research, 48*. <Go to ISI>://WOS:000306905800002

Sokolik, I. N., Toon, O. B., & Bergstrom, R. W. (1998). Modeling the radiative characteristics of airborne mineral aerosols at infrared wavelengths. *Journal of Geophysical Research-Atmospheres, 103*(D8), 8813-8826. <Go to ISI>://WOS:000073290900016

Solmon, F., Nair, V. S., & Mallet, M. (2015). Increasing Arabian dust activity and the Indian summer monsoon. *Atmospheric Chemistry and Physics, 15*(14), 8051-8064. <Go to ISI>://WOS:000358799000019

Tagliabue, A., Aumont, O., DeAth, R., Dunne, J. P., Dutkiewicz, S., Galbraith, E., et al. (2016). How well do global ocean biogeochemistry models simulate dissolved iron distributions? *Global Biogeochemical Cycles, 30*(2), 149-174. <Go to ISI>://WOS:000372963900005

Tang, Q., Klein, S. A., Xie, S., Lin, W., Golaz, J. C., Roesler, E. L., et al. (2019). Regionally refined test bed in E3SM atmosphere model version 1 (EAMv1) and applications for high-resolution modeling. *Geosci. Model Dev., 12*(7), 2679-2706. https://gmd.copernicus.org/articles/12/2679/2019/

Tang, Q., Prather, M. J., Hsu, J., Ruiz, D. J., Cameron-Smith, P. J., Xie, S., & Golaz, J. C. (2021). Evaluation of the interactive stratospheric ozone (O3v2) module in the E3SM version 1 Earth system model. *Geosci. Model Dev., 14*(3), 1219-1236. https://gmd.copernicus.org/articles/14/1219/2021/

Tegen, I., Lacis, A. A., & Fung, I. (1996). The influence on climate forcing of mineral aerosols from disturbed soils. *Nature, 380*(6573), 419-422. <Go to ISI>://WOS:A1996UD59000055

Teixeira, J. C., Carvalho, A. C., Tuccella, P., Curci, G., & Rocha, A. (2016). WRF-chem sensitivity to vertical resolution during a saharan dust event. *Physics and Chemistry of the Earth, Parts A/B/C, 94*, 188-195. http://www.sciencedirect.com/science/article/pii/S1474706515000364

Vinoj, V., Rasch, P. J., Wang, H., Yoon, J.-H., Ma, P.-L., Landu, K., & Singh, B. (2014). Short-term modulation of Indian summer monsoon rainfall by West Asian dust. *Nature Geoscience, 7*(4), 308-313. https://doi.org/10.1038/ngeo2107

Wang, H., Easter, R. C., Zhang, R., Ma, P.-L., Singh, B., Zhang, K., et al. (2020). Aerosols in the E3SM Version 1: New Developments and Their Impacts on Radiative Forcing. *Journal of Advances in Modeling Earth Systems, 12*(1), e2019MS001851. https://agupubs.onlinelibrary.wiley.com/doi/abs/10.1029/2019MS001851

Woodward, S. (2001). Modeling the atmospheric life cycle and radiative impact of mineral dust in the Hadley Centre climate model. *Journal of Geophysical Research-Atmospheres, 106*(D16), 18155-18166. <Go to ISI>://WOS:000170579400036

Wu, M., Liu, X., Yu, H., Wang, H., Shi, Y., Yang, K., et al. (2020). Understanding processes that control dust spatial distributions with global climate models and satellite observations. *Atmos. Chem. Phys., 20*(22), 13835-13855. https://acp.copernicus.org/articles/20/13835/2020/

Xie, S. C., Lin, W. Y., Rasch, P. J., Ma, P. L., Neale, R., Larson, V. E., et al. (2018). Understanding Cloud and Convective Characteristics in Version 1 of the E3SM Atmosphere Model. *Journal of Advances in Modeling Earth Systems, 10*(10), 2618-2644. <Go to ISI>://WOS:000450413200013

Yu, H., Chin, M., Bian, H. S., Yuan, T. L., Prospero, J. M., Omar, A. H., et al. (2015). Quantification of trans-Atlantic dust transport from seven-year (2007-2013) record of CALIPSO lidar measurements. *Remote Sensing of Environment, 159*, 232-249. <Go to ISI>://WOS:000352749000018

Yu, H., Chin, M., Yuan, T. L., Bian, H. S., Remer, L. A., Prospero, J. M., et al. (2015). The fertilizing role of African dust in the Amazon rainforest: A first multiyear assessment based on data from Cloud-Aerosol Lidar and Infrared Pathfinder Satellite Observations. *Geophysical Research Letters, 42*(6), 1984-1991. <Go to ISI>://WOS:000353170000047

Yu, H., Tan, Q., Chin, M., Remer, L. A., Kahn, R. A., Bian, H., et al. (2019). Estimates of African Dust Deposition Along the Trans-Atlantic Transit Using the Decadelong Record of Aerosol Measurements from CALIOP, MODIS, MISR, and IASI. *Journal of Geophysical Research: Atmospheres, 124*(14), 7975-7996. https://doi.org/10.1029/2019JD030574. https://doi.org/10.1029/2019JD030574

Zender, C. S., Bian, H. S., & Newman, D. (2003). Mineral Dust Entrainment and Deposition (DEAD) model: Description and 1990s dust climatology. *Journal of Geophysical Research-Atmospheres, 108*(D14). <Go to ISI>://WOS:000184611000001

Zhang, K., Zhao, C., Wan, H., Qian, Y., Easter, R. C., Ghan, S. J., et al. (2016). Quantifying the impact of sub-grid surface wind variability on sea salt and dust emissions in CAM5. *Geosci. Model Dev., 9*(2), 607-632. https://www.geosci-model-dev.net/9/607/2016/

Zhang, L., Gong, S., Padro, J., & Barrie, L. (2001). A size-segregated particle dry deposition scheme for an atmospheric aerosol module. *Atmospheric Environment, 35*(3), 549-560. https://www.sciencedirect.com/science/article/pii/S1352231000003265

Zhao, A., Ryder, C. L., & Wilcox, L. J. (2021). How well do the CMIP6 models simulate dust aerosols? *Atmos. Chem. Phys. Discuss., 2021*, 1-32. https://acp.copernicus.org/preprints/acp-2021-578/

Zhao, C., Chen, S., Leung, L. R., Qian, Y., Kok, J. F., Zaveri, R. A., & Huang, J. (2013). Uncertainty in modeling dust mass balance and radiative forcing from size parameterization. *Atmos. Chem. Phys., 13*(21), 10733-10753. https://www.atmos-chem-phys.net/13/10733/2013/

Zhao, C., Liu, X., & Leung, L. R. (2012). Impact of the Desert dust on the summer monsoon system over Southwestern North America. *Atmospheric Chemistry and Physics, 12*(8), 3717-3731. <Go to ISI>://WOS:000304054800011

Zhao, C., Liu, X., Leung, L. R., & Hagos, S. (2011). Radiative impact of mineral dust on monsoon precipitation variability over West Africa. *Atmospheric Chemistry and Physics, 11*(5), 1879-1893. <Go to ISI>://WOS:000288368900003

Zhu, A., Ramanathan, V., Li, F., & Kim, D. (2007). Dust plumes over the Pacific, Indian, and Atlantic oceans: Climatology and radiative impact. *Journal of Geophysical Research-Atmospheres, 112*(D16). <Go to ISI>://WOS:000249335400002

Table 1 Description of the E3SMv1 (or EAMv1) model simulations included

#	Simulation	Horizontal resolution	Vertical layers	Results	Physics parameter tuning	Dust size distri.	SW optics	DAOD/ AOD	DRE
(1)	LRes (EAMv1)	~1°	72	Years 2-11 (cold start)	FC5AV1C -04P2	Default	Default	0.029/ 0.142	Yes
	Sensitivity experiments to dust properties, nudging and high-resolution parameter tuning								
(2)	LResT	~1°	72	Years 2-11 (cold start)	FC5AV1C -04P2	Kok (2011)	AERO NET	0.029/ 0.141	Yes
(3)	LResT-Ndg	~1°	72	2010 (nudging, initialized from the 2009 run)	FC5AV1C -04P2	Kok (2011)	AERO NET	0.026/ 0.135	No
(4)	LResT-Ndg-HRtuned	~1°	72	2010 (nudging, initialized from the 2009 run)	FC5AV1C -H01A	Kok (2011)	AERO NET	0.026/ 0.129	No
	Sensitivity experiments to resolution								
(5)	HRes (EAMv1)	~0.25°	72	Years 2-5 (cold start)	FC5AV1C -H01A	Default	Default	0.032/ 0.135	No
(6)	LResZ30	~1°	30	Years 2-6 (cold start)	FC5AV1C -04P2	Default	Default	0.029/ 0.145	No
	Resolution effect on direct radiative effect								
(7)	LResT-HRtuned	~1°	72	Year 2 (cold start)	FC5AV1C -H01A	Kok (2011)	AERO NET	0.038/ 0.149	Yes
(8)	HResT	~0.25°	72	Year 2 (cold start)	FC5AV1C -H01A	Kok (2011)	AERO NET	0.04/ 0.147	Yes

Table 2 Location of the selected 19 AERONET dusty sites and annual mean AOD and AAOD from the E3SM model (LRes, LResT, and LResT-Ndg) and AERONET (Obs). Also shown are the calculated Pearson's correlation coefficients between the AERONET (Obs) data and model calculations

Site	Lat.	Lon.	**Obs**	LRes	LResT	LResT-Ndg	**Obs**	LRes	LResT	LResT-Ndg
				AOD				AAOD		
Trelew	-43.25	294.69	**0.036**	0.035	0.036	0.033	**0.005**	0.002	0.002	0.002
Tinga_Tingana	-28.98	139.99	**0.042**	0.134	0.138	0.108	**0.005**	0.014	0.009	0.007
DMN_Maine_Soroa	13.22	12.02	**0.466**	0.742	0.799	0.768	**0.038**	0.090	0.054	0.050
IER_Cinzana	13.28	354.07	**0.436**	0.475	0.467	0.397	**0.025**	0.051	0.030	0.025
Banizoumbou	13.55	2.67	**0.482**	0.591	0.600	0.522	**0.023**	0.067	0.039	0.033
Dakar	14.39	343.04	**0.445**	0.487	0.467	0.402	**0.023**	0.052	0.030	0.026
Agoufou	15.35	358.52	**0.461**	0.493	0.489	0.421	**0.022**	0.056	0.031	0.026
Hada_El-Sham	21.80	39.73	**0.358**	0.304	0.290	0.315	**0.007**	0.034	0.020	0.022
KAUST_Campus	22.30	39.10	**0.379**	0.313	0.303	0.323	**0.015**	0.036	0.021	0.023
Tamanrasset_INM	22.79	5.53	**0.249**	0.284	0.285	0.327	**0.014**	0.033	0.019	0.021
Masdar_Institute	24.44	54.62	**0.369**	0.335	0.342	0.312	**0.018**	0.039	0.024	0.023
Solar_Village	24.91	46.40	**0.395**	0.271	0.269	0.288	**0.024**	0.031	0.019	0.021
Karachi	24.95	67.14	**0.435**	0.295	0.300	0.392	**0.030**	0.030	0.020	0.026
Dhadnah	25.51	56.32	**0.359**	0.340	0.351	0.305	**0.024**	0.040	0.024	0.022
El_Farafra	27.06	27.99	**0.191**	0.343	0.363	0.352	**0.009**	0.043	0.026	0.026
Santa_Cruz_Tenerife	28.47	343.75	**0.154**	0.221	0.206	0.166	**0.005**	0.017	0.010	0.007
Ouarzazate	30.93	353.09	**0.140**	0.154	0.153	0.177	**0.010**	0.016	0.010	0.012
Saada	31.63	351.84	**0.206**	0.155	0.154	0.166	**0.012**	0.016	0.010	0.011
Medenine-IRA	33.50	10.64	**0.163**	0.421	0.467	0.520	**0.008**	0.052	0.031	0.036
Multi-site mean			**0.30**	0.34	0.34	0.33	**0.017**	0.038	0.023	0.022
Correlation: Obs vs				(0.77)	(0.72)	(0.70)		(0.72)	(0.74)	(0.71)

Table 3 Comparisons of dust annual deposition fluxes (g m^{-2} yr^{-1}) by region. The observational data are taken from Albani et al. (2014). Also shown are the regional mean deposition fluxes from LRes, LResT and HRes as well as the ratios over the observational data (numbers in parentheses)

Region (# of sites)	Observations	LRes	LResT	HRes
N Africa/Sub. Atlantic (27)	12	24.7 (2.1)	32.8 (2.7)	28.4 (2.4)
Europe/N. Atlantic (13)	6.4	5.9 (0.9)	6.5 (1.)	6.41 (1.)
Asia/Arabian Sea (15)	26	38.7 (1.5)	52 (2.0)	51.4 (2.0)
N. America (2)	1.9	1.7 (0.9)	2.3 (1.2)	2.76 (1.5)
N Pacific (15)	2.3	1.15 (0.5)	1.25 (0.5)	1.55 (0.7)
S Atlantic/S. America (6)	7.7	5.3 (0.7)	7.14 (0.9)	6.82 (0.9)
S Pacific/Australia (13)	1.4	0.67 (0.5)	0.86 (0.6)	1.11 (0.8)
Antarctica (15)	0.003	0.06 (19.1)	0.08 (23.9)	0.02 (5.2)
Arctic (2)	0.029	0.07 (2.4)	0.08 (2.6)	0.08 (2.8)
All the sites (108):	8.35	12.8 (1.5)	16.9 (2.0)	15.8 (1.9)

Table 4 Global budgets for dust in E3SMv1 (LRes, LResT, LResT-Ndg, HRes, and LResZ30) compared with CAM5 and other modeling studies

	E3SMv1					CAM5	Other studies
	LRes	LResT	LResT-Ndg	HRes	LResZ30		
Horizontal Res	1°	1°	1°	0.25°	1°	1.9°	Variable
Vertical layers	72	72	72	72	30	30	Variable
Emission (Tg/yr)	4377	5921	5256	4751	4173	3122	1840±49%
Deposition (Tg/yr):							
Dry	3385(0.42)	4657(0.46)	4088(0.41)	3320(0.35)	2948(0.29)	(0.24)	(0.23±84%)
Wet	990(0.12)	1260(0.12)	1160(0.12)	1331(0.14)	1298(0.13)	(0.14)	(0.08±42%)
Burden (Tg)	22.2	27.9	27.1	27.0	28.3	22.4	19.2±40%
Lifetime (day)	1.85	1.72	1.88	2.1	2.4	2.6	4.14±43%
Dust AOD	0.029	0.029	0.029	0.032	0.029	0.033	0.023

*Note. The numbers in parentheses are calculated dry (or wet) deposition rate in unit of day^{-1}, defined as dry (or wet) deposition flux divided by burden*365 in Textor et al. (2006). Also shown are the model outputs from CAM5 (Scanza et al., 2015). The means and normalized standard deviations (in %) of the "Other studies" are taken from Liu et al. (2012) except for dust AOD from Huneeus et al. (2011)*

Table 5 Annual and global mean radiation budgets in E3SMv1 (LRes, LResT, LResT-HRtuned, HResT and HResT*). Also shown are the global DAOD and AOD associated with the estimated radiative fluxes.

	DAOD	AOD	TOA (W m^{-2})			Atmosphere (W m^{-2})			Surface (W m^{-2})		
			SW	LW	**NET**	SW	LW	**NET**	SW	LW	**NET**
LRes	0.029	0.142	-0.16	0.08	**-0.08**	1.35	-0.34	**1.01**	-1.51	0.42	**-1.09**
LResT	0.029	0.141	-0.52	0.1	**-0.42**	0.68	-0.44	**0.24**	-1.20	0.54	**-0.65**
LResT-HRtuned	0.038	0.149	-0.74	0.14	**-0.6**	0.99	-0.65	**0.35**	-1.73	0.79	**-0.95**
HResT	0.04	0.147	-0.73	0.16	**-0.58**	1.08	-0.71	**0.37**	-1.81	0.87	**-0.95**
HResT*	0.029		-0.53	0.12	**-0.42**						

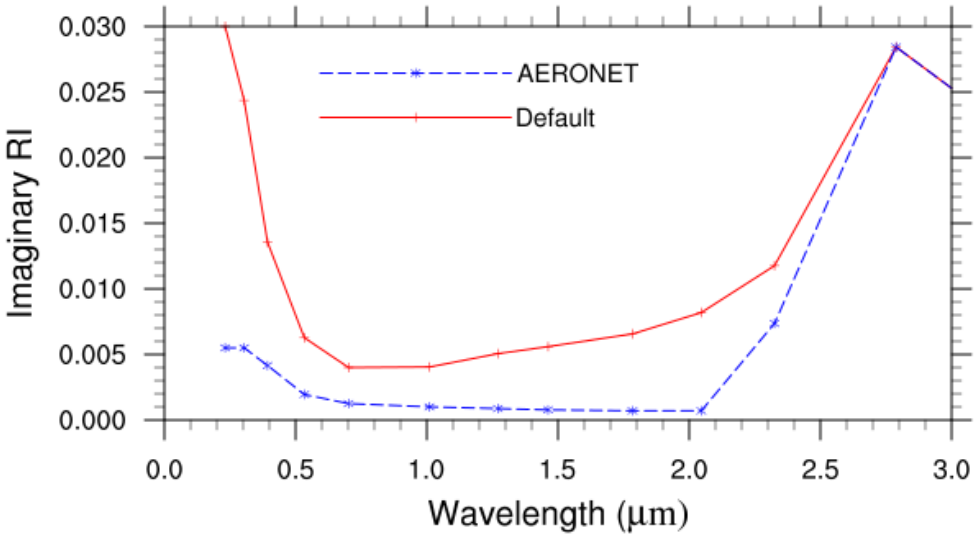

Figure 1. Dust imaginary refractive indices (RI) in the default E3SM model and sensitivity studies of this work based on the AERONET measurements

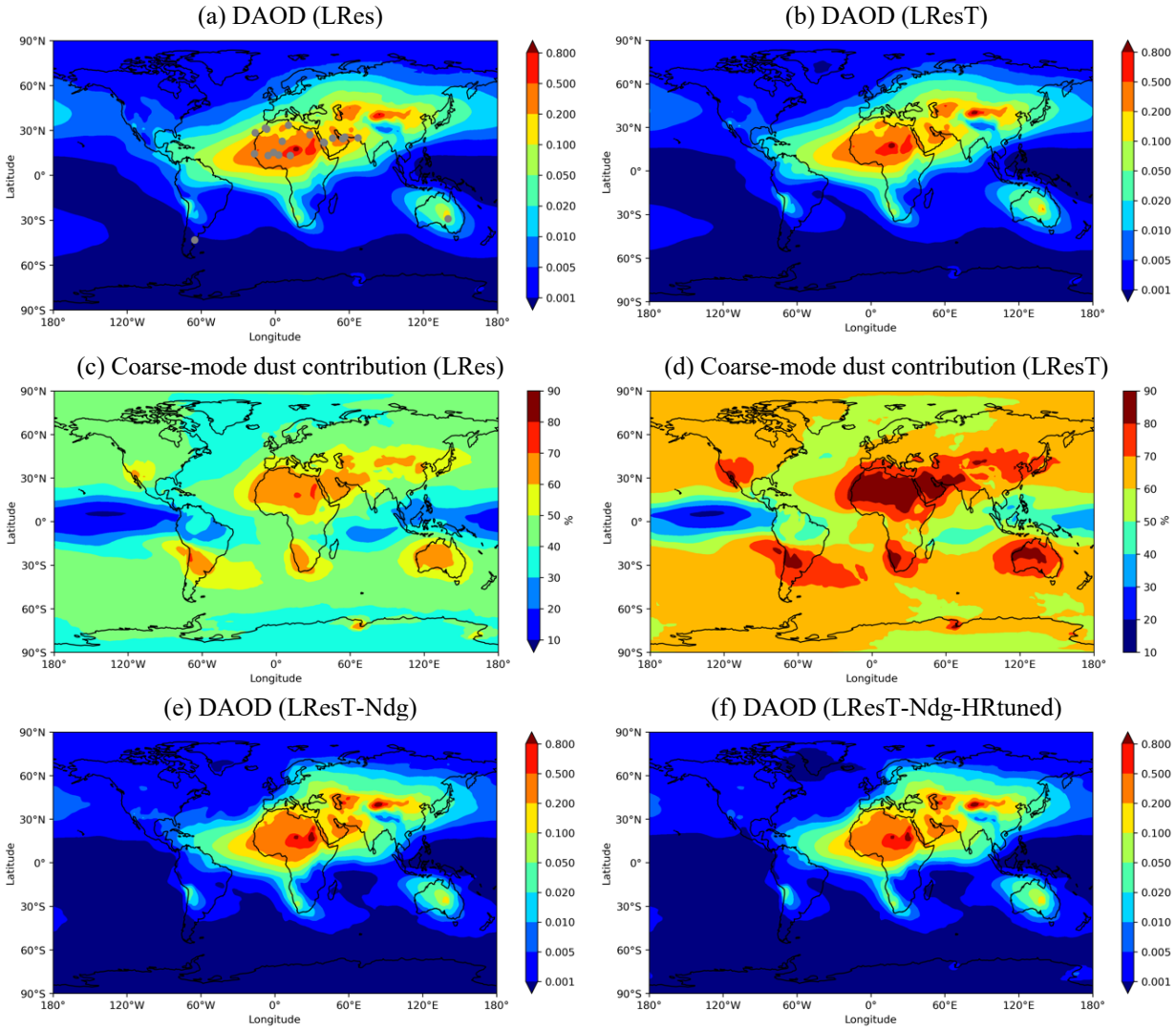

Figure 2. Annual mean dust aerosol optical depth (DAOD) at 550nm predicted by the low-resolution E3SMv1 with the (a) default configuration (LRes) and (b) updated dust physics (LResT). Contribution (%) of the coarse-mode dust in total DAOD is shown for (c) LRes and (d) LResT, respectively. Also shown are the annual mean DAOD distributions from the two sensitivity studies: (e) LResT-Ndg and (f) LResT-Ndg-HRtuned. Grey circles in the panel (a) indicate the 19 'dusty' AERONET sites selected

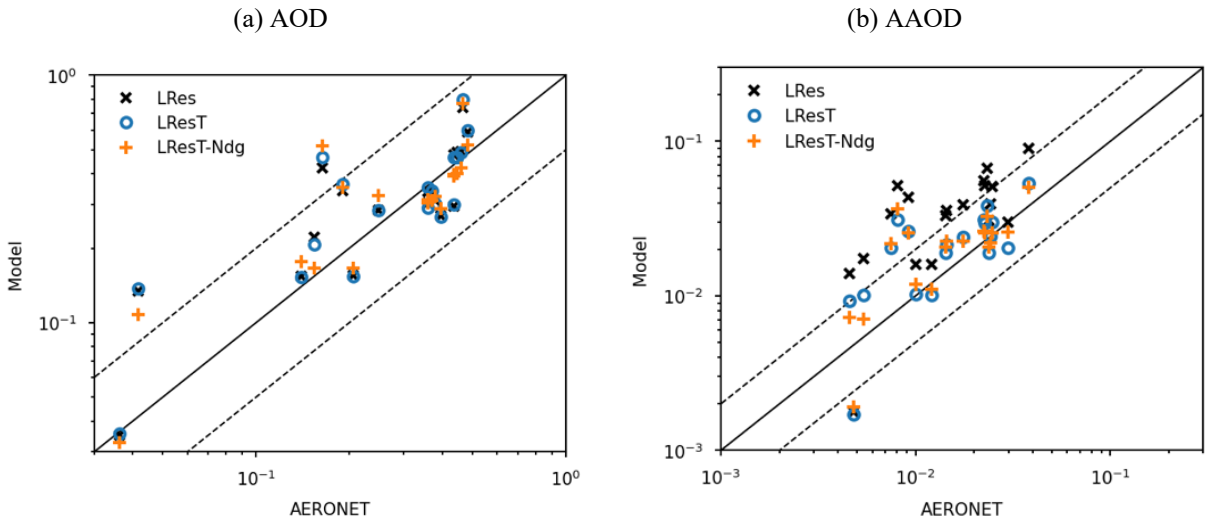

Figure 3. Annual mean (a) AOD and (b) AAOD comparison with the AERONET data over the selected dusty sites. Results from the LRes (cross symbols), LResT (open circles), and LResT-Ndg (plus symbols) simulations are shown. The black solid line represents the 1:1 line and the dash lines are for the 1:2 and 2:1 ratios

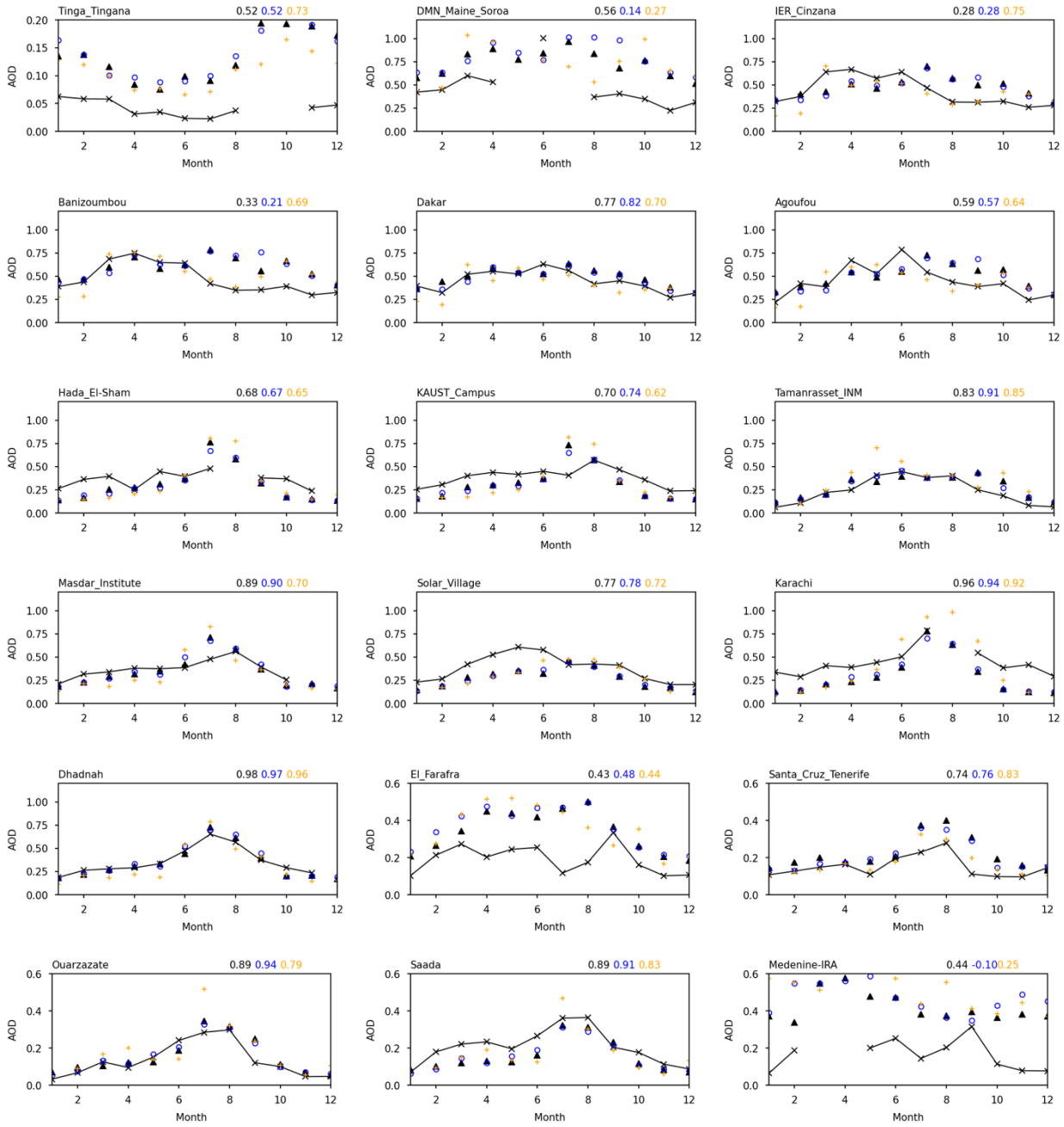

Figure 4. Seasonal variations of monthly AODs over the 18 dusty AERONET sites simulated by LRes (triangle), LResT (blue circle), and LResT-Ndg (orange plus), compared with the AERONET data (line with cross symbols). The site name and calculated Pearson correlation coefficients between LRes (black), LResT (Blue), LResT-Ndg (orange) and observations are shown on top of each panel. The AERONET site information is given in Table 2

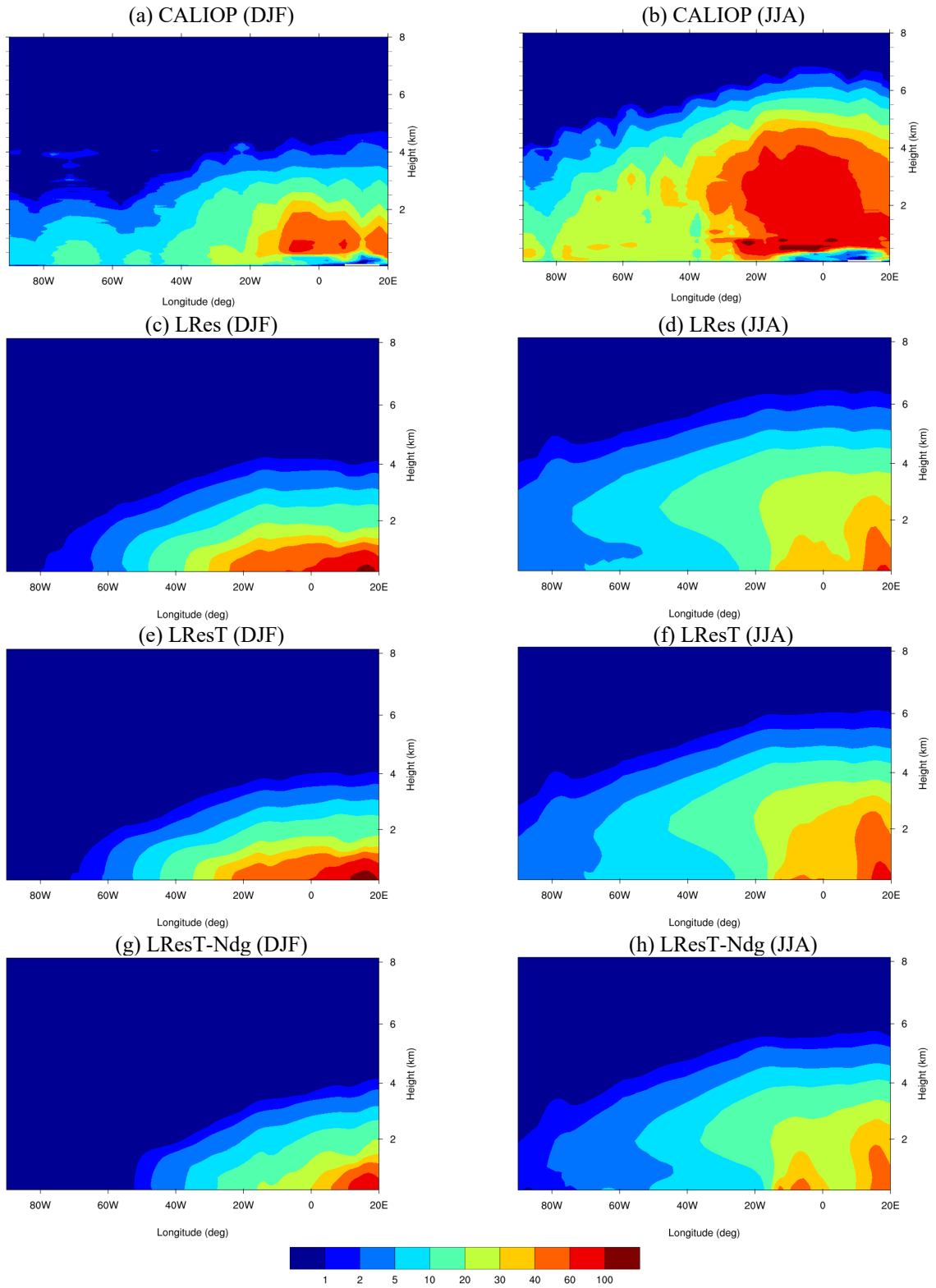

Figure 5. Crosssection of dust extinctions (Mm^{-1}) averaged between 0 and 30°N for winter (DJF: December-January-February), and summer (JJA: June-July-August), as shown in (a) and (b) for the CALIOP retrievals in year 2010, compared with the E3SM simulations in (c) and (d) from LRes, (e) and (f) from LResT, and (g) and (h) from LResT-Ndg

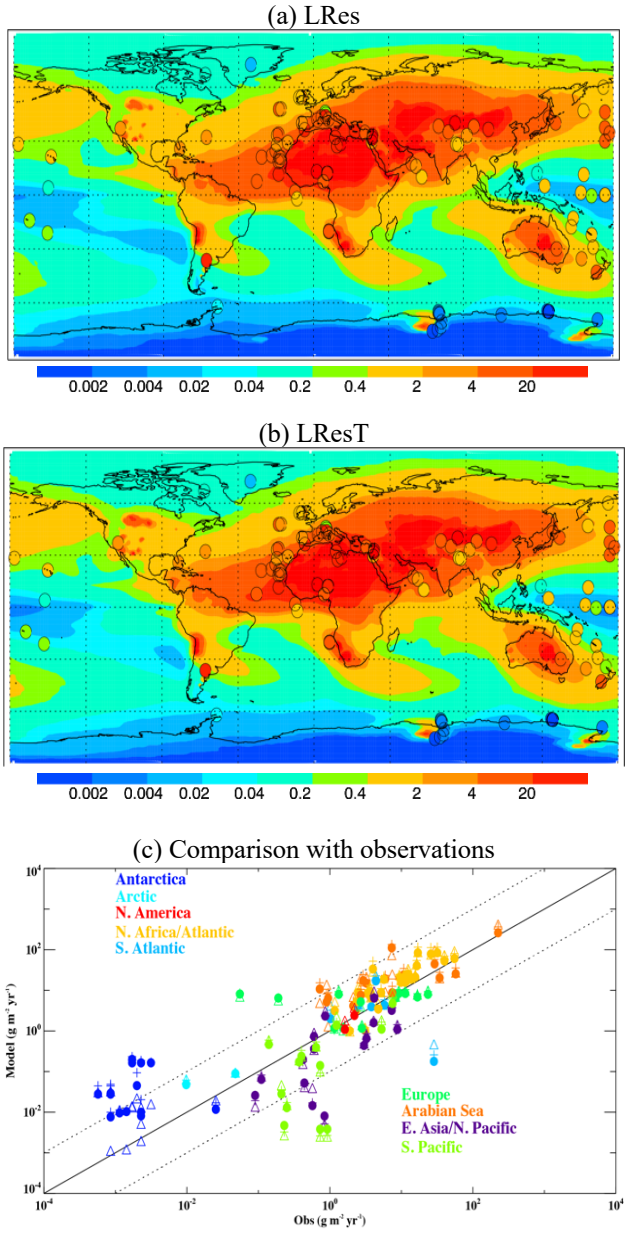

Figure 6. Spatial distribution of annual dust deposition flux (g m^{-2} yr^{-1}) from (a) LRes and (b) LResT. Observational data over 108 locations are overlaid by filled circles with values shown in the same colour scale. Panel (c) compares the model results from LRes (solid circles), LResT (plus symbols), and HRes (open triangles) with the data at the observational sites. The black solid line represents the 1:1 line and the dash lines are for the 1:10 and 10:1 ratios

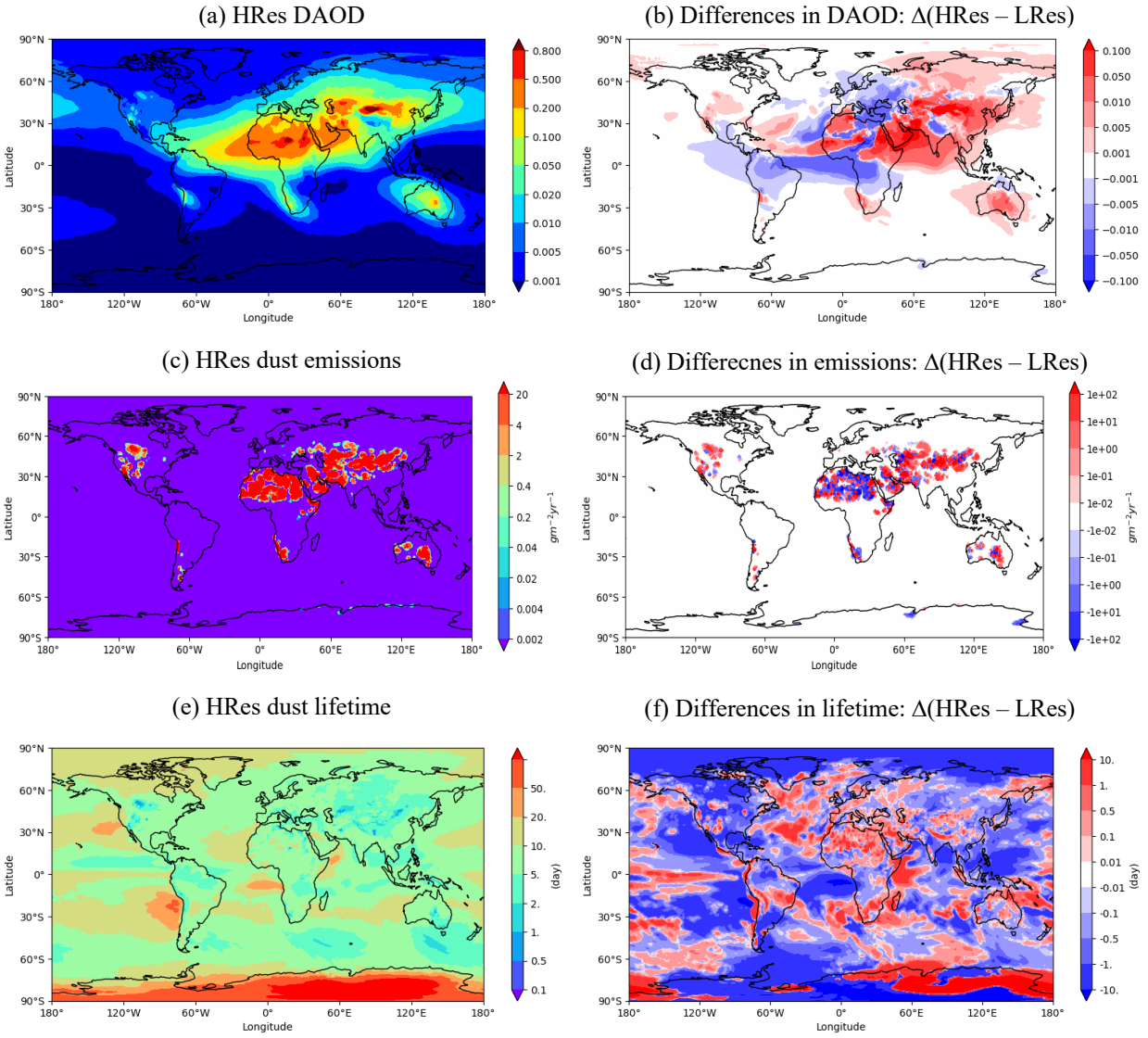

Figure 7. HRes simulations of (a) annual mean DAOD at 550nm, (c) dust emissions (g m^{-2} yr^{-1}), and (e) lifetime (day). Also shown are the differences between the HRes and LRes simulations in (b) DAOD, (d) dust emissions (g m^{-2} yr^{-1}), and (f) lifetime (day)

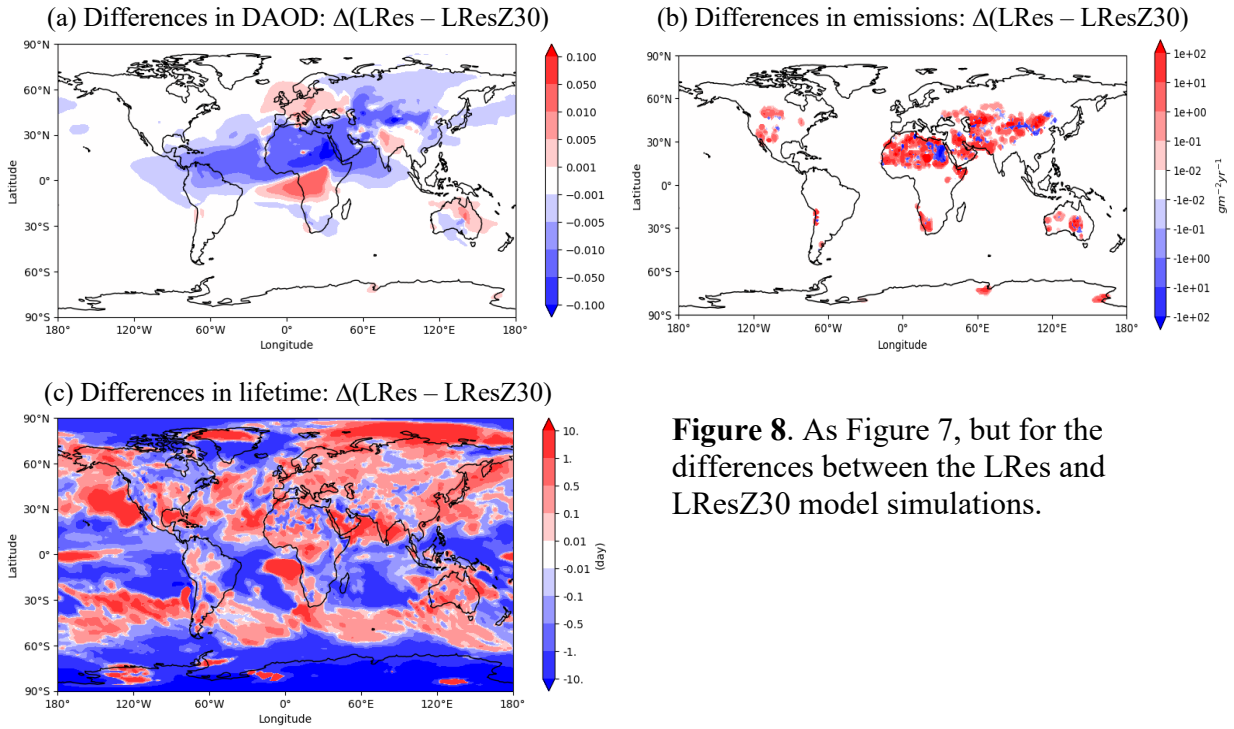

Figure 8. As Figure 7, but for the differences between the LRes and LResZ30 model simulations.

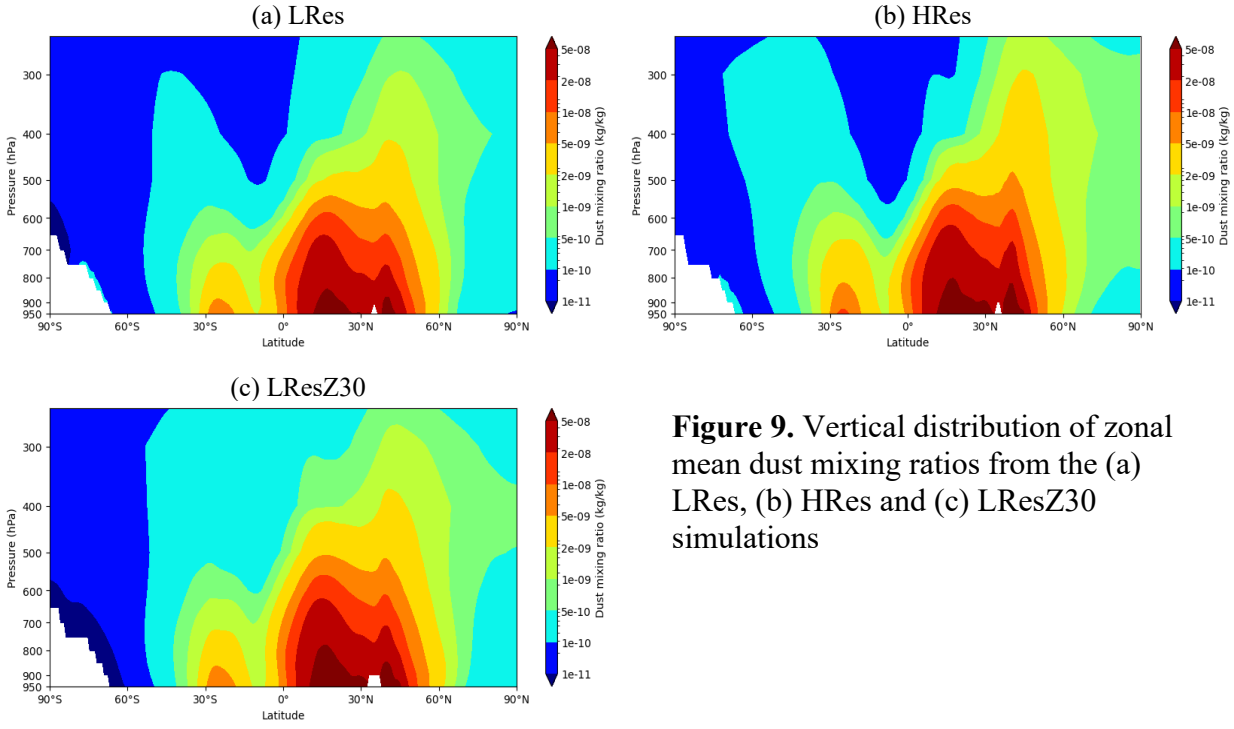

Figure 9. Vertical distribution of zonal mean dust mixing ratios from the (a) LRes, (b) HRes and (c) LResZ30 simulations

(a) Δ(HRes – LRes)

(b) Δ(LRes – LResZ30)

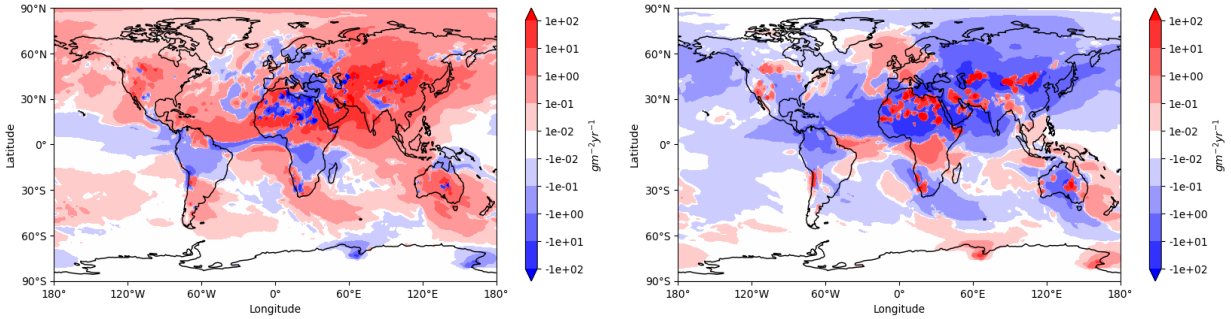

Figure 10. Differences in simulated annual dust deposition fluxes (g m^{-2} yr^{-1}) between (a) HRes and LRes: Δ(HRes – LRes) and (b) LRes and LResZ30: Δ(LRes – LResZ30)

(a) LRes

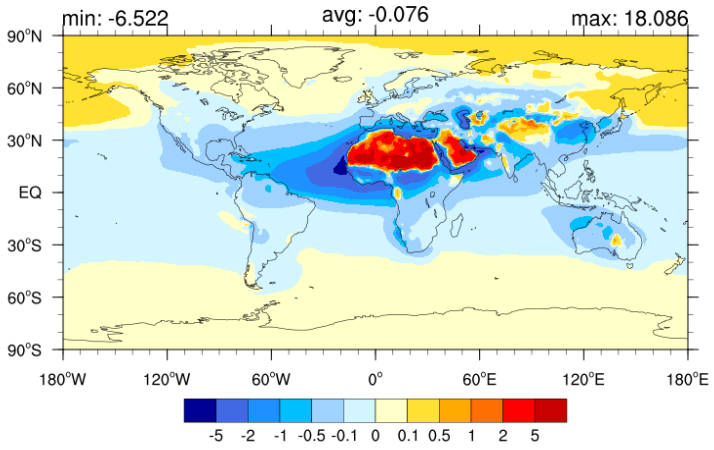

(b) LResT

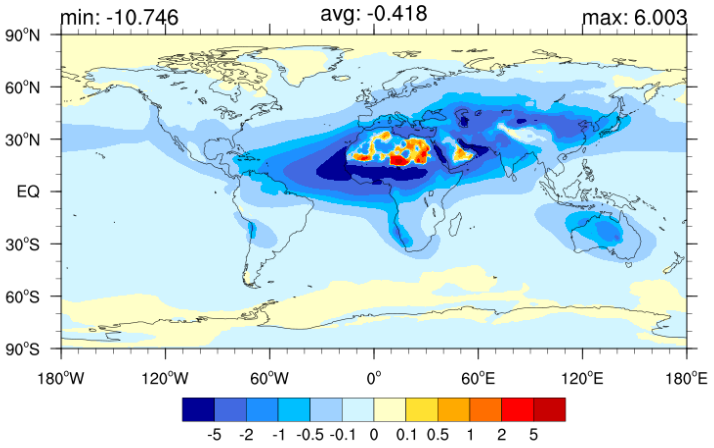

(c) HResT – LResT_HRtuned

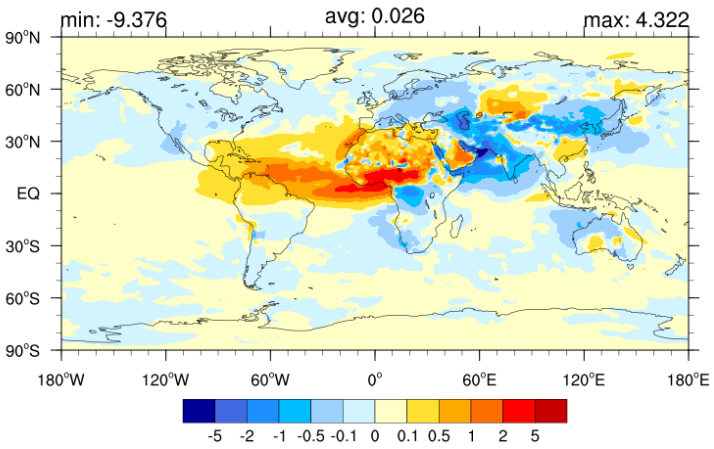

Figure 11. Dust direct radiative effect (W m^{-2}) at the top of the atmosphere from (a) LRes (EAMv1 low resolution), (b) LResT (this work), and (c) HResT-LResT_HRtuned (impact of higher horizontal resolution)

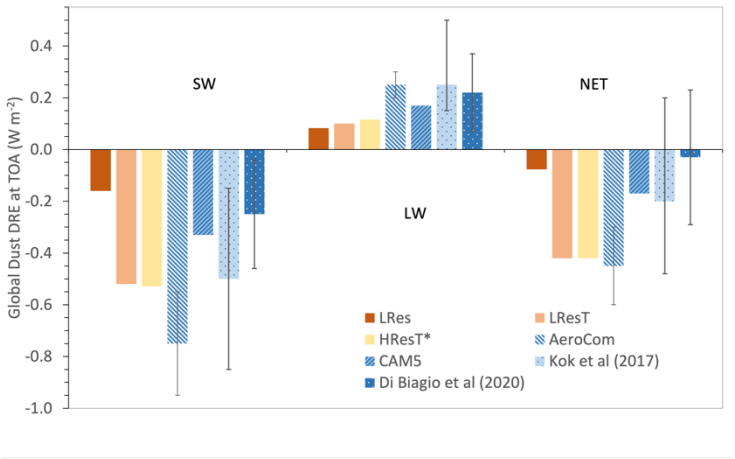

Figure 12. Comparison of the estimated dust direct radiative effects (DRE: W m^{-2}) at the top of the atmosphere (TOA) for for the shortwave (SW), longwave (LW), and net effects (NET), respectively, from the E3SM simualtions (LRes, LResT, and HResT*). HResT* denotes the HResT DREs, whose values are normalized to the LRes DAOD. Also shown are the results from CAM5 (Scanza et al., 2015), Di Biagio et al. (2020), and Kok et al. (2017) which also include the published AeroCom model estimates